

Orally Effective Aminoalkyl 10*H*-Indolo[3,2-*b*]quinoline-11-carboxamide Kills the Malaria Parasite by Inhibiting Host Hemoglobin Uptake

Ramesh Mudududdla^{+, [a]} Dinesh Mohanakrishnan^{+, [b]} Sonali S. Bharate,^[a]
Ram A. Vishwakarma,^[a] Dinkar Sahal,^{*, [b]} and Sandip B. Bharate^{*, [a]}

A series of indolo[3,2-*b*]quinoline-C11-carboxamides were synthesized by incorporation of aminoalkyl side chains into the core of indolo[3,2-*b*]quinoline-C11-carboxylic acid. Their in vitro antiparasitic evaluation against *Plasmodium falciparum* led to the identification of a 2-(piperidin-1-yl)ethanamine-linked analogue {2-bromo-*N*-[2-(piperidin-1-yl)ethyl]-10*H*-indolo[3,2-*b*]quinoline-11-carboxamide (**3g**)} (IC₅₀ = 1.3 μM) as the most promising compound exhibiting good selectivity indices against mammalian cell lines. The kill kinetics on erythrocytic-stage parasites revealed that **3g** caused complete killing of only the trophozoite-stage parasites. Mechanistic studies

showed that **3g** targets the food vacuole of the parasite and inhibits hemoglobin uptake, β-hematin formation, and the basic endocytic processes of the parasite. Analogue **3g** was found to be orally bioavailable, and its curative antimalarial studies at 50 mg per kg p.o. against a *Plasmodium berghei* (ANKA)-infected mouse model revealed that mice treated with **3g** showed 27–35% suppression of parasitemia with an increase in life span relative to untreated, control mice. Thus, the present work demonstrated a proof of concept for the oral efficacy of indolo[3,2-*b*]quinoline-C11-carboxamides.

Introduction

Malaria is a parasitic disease transmitted to humans by the bites of infected female anophelid mosquito. Five species of *Plasmodium* (*P. falciparum*, *P. vivax*, *P. ovale*, *P. malariae*, and *P. knowlesi*) are known to cause malaria; *P. falciparum* and *P. vivax* are the most common, but *P. falciparum* has a major impact, as it is responsible for the largest number of malarial deaths in humans. In 2016, approximately 216 million cases and 445 000 malaria associated deaths were reported around the world, mostly among African children below 5 years of age.^[1] Several medications for the treatment of malaria are known, including 4-aminoquinolines [e.g., chloroquine (CQ)], artemisinin derivatives (e.g., artemether), tetracyclines, and also several combination therapies. Over the last several decades, front-line antimalarial drugs, that is, chloroquine, antifolates, and artemisinin, have been losing their efficacy owing to the

emergence of resistance.^[2] To overcome parasitic resistance, there is a need to find more effective new antimalarial drugs. Currently, several research groups are working toward the discovery of more efficient antimalarial drugs, and several clinical studies are in progress.^[3] Nature has been valuable in providing drugs against malaria (e.g., quinine and artemisinin are secondary metabolites of plants) and continues to be the best repository for druggable lead compounds against several diseases, including malaria.^[4]


Since ancient times, plants and plant-derived natural products have been used as remedies for various illnesses. Alkaloids have contributed significantly to antimalarial drug discovery, and currently, a large number of alkaloids are in clinic or in clinical development.^[5] Indoloquinoline alkaloids are naturally occurring fused cyclic compounds that can be isolated from the West African climbing shrub *Cryptolepis sanguinolenta*.^[6] The roots of this plant are used as a folk medicine in central and West Africa as an antirheumatic and spasmolytic and for the treatment of malaria, bacterial infection, hepatitis, and so on.^[7] This plant was first studied in 1929,^[8] at which point the major chemical constituent, cryptolepine (**1**), was isolated. In 1951, Gellért et al.^[9] assigned the exact chemical structure of cryptolepine as a linearly fused 5-methyl-10*H*-indolo[3,2-*b*]quinoline.

Cryptolepine (**1**) is reported to possess antimalarial activities against both CQ-sensitive and CQ-resistant strains^[10] and is also endowed with anticancer,^[11] anti-hyperglycemic,^[12] anti-bacterial/antifungal,^[13] and anti-infective activities.^[14] The cytotoxic properties of cryptolepine are due to DNA intercalation by binding of the N5 quaternary methyl group at cytosine-cy-

[a] Dr. R. Mudududdla,⁺ Dr. S. S. Bharate, Dr. R. A. Vishwakarma,
Dr. S. B. Bharate
CSIR-Indian Institute of Integrative Medicine, Canal Road, Jammu 180001
(India)
E-mail: sbharate@iiim.ac.in
Homepage: www.iiim.res.in

[b] Dr. D. Mohanakrishnan,⁺ Dr. D. Sahal
Malaria Drug Discovery Laboratory, International Centre for Genetic Engineering and Biotechnology (ICGEB), Aruna Asaf Ali Marg, New Delhi 110067
(India)
E-mail: dinkar@icgeb.res.in

[⁺] These authors contributed equally to this work.

 Supporting Information (NMR spectra of all compounds) and the ORCID identification number(s) for the author(s) of this article can be found under:
<https://doi.org/10.1002/cmdc.201800579>.

tosine sites, which causes inhibition of DNA synthesis.^[11,15] However, the high cytotoxicity and low selectivity of this alkaloid have prevented it from clinical development for the treatment of malaria.^[16] Several studies^[17] have shown that the incorporation of basic amino functionalities at the C11 position (e.g., structure **2**, Figure 1) in the scaffold of cryptolepine en-

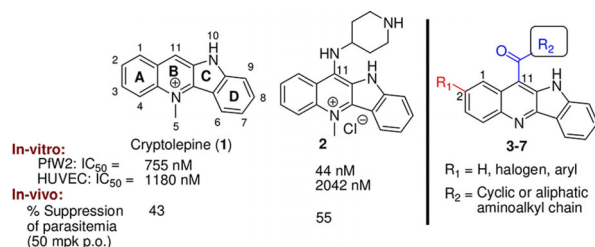


Figure 1. Structures of cryptolepine (**1**), C11-substituted analogue **2**, and C11 carboxamides **3–7**.

hances the antimalarial potency. Cryptolepine shows antiparasmodial activity against the *P. falciparum* W2 strain with an IC₅₀ value of 755 nM and cytotoxicity in the HUVEC cell line with a CC₅₀ value of 1180 nM. The incorporation of a 4-piperidinamino group at C11 (in the cryptolepine structure) results in a 17-fold improvement in antiparasmodial activity (compound **2**, PW2: IC₅₀ = 44 nM) and reduced cytotoxicity in HUVEC cells (CC₅₀ = 2042 nM). Cryptolepine (**1**) and compound **2** at 50 mg/kg/day (p.o.) suppress parasitemia in mice by 43 and 55%.^[18] The effect of C11 carboxamide-linked aminoalkyl chains has never been investigated. Furthermore, the cytotoxicity of this class of compounds is primarily associated with their planar structures and quaternary nitrogen atoms; therefore, considering these structural aspects, herein we designed a new series of indoloquinolines (i.e., compounds **3–7**) comprising a saturated aminoalkyl linker at the C11 position to maintain (or to improve) antimalarial activity and a non-quaternary quinoline nitrogen atom. The synthesized compounds were tested for their antiparasmodial activity against CQ-sensitive and CQ-resistant strains of *P. falciparum*.

The preclinical parameters (including aqueous solubility, cytochrome P450 enzyme inhibition, caco-2 permeability) of the best-identified compound were determined, which was followed by oral pharmacokinetics and in vivo antimalarial efficacy. The detailed studies performed to understand the mechanism of antimalarial action of fluorescent lead compound **3g** revealed that it targets the food vacuole, at which it inhibits the uptake of hemoglobin and inhibits the detoxification of heme to hemozoin.

Results and Discussion

Chemistry

Cryptolepine (**1**) was synthesized starting from commercially available anthranilic acid (**8**), as depicted in Figure 2A.^[12,17a] Reaction of anthranilic acid (**8**) with bromoacetyl bromide gave *N*-bromoacetyl anthranilic acid (**9**), which on coupling with ani-

line under reflux conditions produced compound **10**. Compound **10** was cyclized by using polyphosphoric acid (PPA) at 140 °C to give indolo[3,2-*b*]quinolin-11-one **11**. The POCl₃-mediated chlorination of **11** gave 11-chloro-10*H*-indolo[3,2-*b*]quinoline (**12**). Hydrogenation of **12** was performed by using H₂/Pd in AcOH and NaOAc at 60 psi to give 10*H*-indolo[3,2-*b*]quinoline (**13**). The final step of *N*-methylation was done by treating **13** with methyl iodide in MeCN under reflux to yield cryptolepine iodide (**1**) as an orange-yellow solid.

For the synthesis of the C11 cryptolepine carboxamide series of compounds, we proposed two major modifications to the scaffold of cryptolepine (**1**). First, with the aim to enhance antiparasmodial potency, we planned to incorporate various carboxamide-linked aminoalkyl side chains at the C11 position of quinoline. In a second modification aimed at reducing the toxicity, we planned to remove the quaternary methyl group of cryptolepine. Key C11 COOH intermediates **18a–d** were prepared starting from anthranilic acid (**8**) in four steps, as depicted in Figure 2B. The reaction of anthranilic acid (**8**) with chloroacetic acid in basic medium yielded 2-[(carboxymethyl)amino]benzoic acid (**14**), which upon *N*-acetylation by using Ac₂O produced 2-[*N*-(carboxymethyl)acetamido]benzoic acid (**15**). Cyclization of **15** was done by acetic anhydride and triethylamine to give 1-acetyl-1*H*-indol-3-yl acetate (**16**). Next, base-mediated cyclization of acetate **16** with isatins **17a–d** produced substituted indolo[3,2-*b*]quinoline-C11-carboxylic acids **18a–d**. Treatment of C11 carboxylic acid derivatives **18a–d** with aliphatic three-to-four carbon-chain amines **19** in the presence of 3-[bis(dimethylamino)methyl]triethylamine (HBTU)/diisopropylethylamine (DIEA) as a peptide coupling agent produced compounds **3a–n**. Suzuki coupling of 2-bromo compound **3a** with arylboronic acids **20a–c** by using [1,1'-bis(diphenylphosphino)ferrocene]dichloropalladium(II) [Pd(dppf)Cl₂] produced 2-aryl-C11-carboxamide derivatives **4a–c**. Similarly, treatment of C11 carboxylic acid intermediates **18a–d** with secondary amines **21** produced carboxamides **5a–h**. Furthermore, treatment of **18a–d** with benzylamines **22a–c** and anilines **23a–c** produced carboxamides **6a–c** and **7a–c**, respectively. All newly synthesized derivatives were fully characterized by ¹H NMR and ¹³C NMR spectroscopy in addition to MS, and their purity was checked by HPLC and LC-HRMS (ESI) analysis.

In vitro antiparasmodial activity

Synthesized compounds **3a–n**, **4a–c**, **5a–h**, **6a–c**, and **7a–c** were all screened for their in vitro antiparasmodial activity against CQ-sensitive (3D7) and CQ-resistant (Dd2 and Indo) strains of *P. falciparum*. To assess the ability of these compounds to kill *Plasmodium* parasites selectively, the cytotoxicity of all compounds was checked in two mammalian cell lines: HUH-7 and HEK-293T (Table 1). Compounds **3a–n** from the first series bearing a C2 halo group and a C11 aliphatic amino carboxamide moiety showed promising antiparasmodial activity against both CQ-sensitive and CQ-resistant strains. Piperidiny-ethyl carboxamide analogue **3g** displayed antiparasmodial activity against *P. falciparum* 3D7, Dd2, and Indo strains with IC₅₀

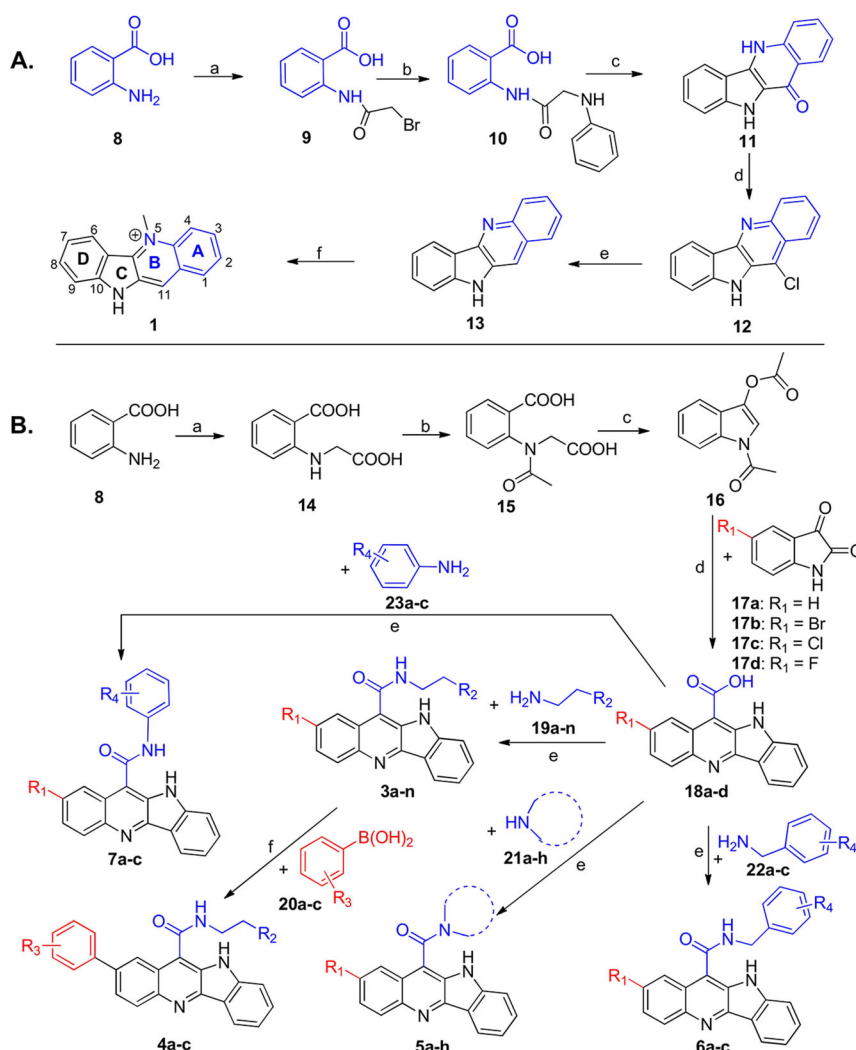


Figure 2. A) Synthesis of cryptolepine (**1**): a) bromoacetyl bromide (1.2 equiv), 1,4-dioxane/DMF (1:1), 18 h, 82%; b) aniline (1.2 equiv), DMF, 130 °C, 85%; c) PPA (excess), 130 °C, 2 h, 67%; d) POCl₃ (excess), 2 h, 60%; e) H₂/10% Pd/C, AcOH, NaOAc, 60 psi, 2 h, 80%; f) CH₃I, DMF, 80 °C, 12 h, 70%. B) Synthesis of indolo[3,2-*b*]quinoline-11-carboxamides **3–7**: a) chloroacetic acid (1.1 equiv), Na₂CO₃ (5.0 equiv), H₂O, 18 h, 82%; b) Ac₂O (1.2 equiv), Na₂CO₃ (1.0 equiv), DMF, 80–85%; c) Ac₂O (10.0 equiv), Et₃N (3.0 equiv), 100 °C, 2 h, 80%; d) KOH (2.0 equiv), H₂O, 6 h, reflux, 70–80%; e) HBTU (1.2 equiv), DIEA (3 equiv), DMF, 6 h, 40–60%; f) Pd(dppf)Cl₂ (0.2 equiv), 1,4-dioxane/H₂O, 80 °C, 12 h, 60–80%.

values of 1.3, 6.3, and 5 μ m and with resistance indices of 4.8 (Dd2/3D7) and 3.8 (INDO/3D7). Also, derivative **3g** showed good selectivity indices of 47 and 33 against HUH-7 and HEK-293T, respectively. The replacement of the C2 halo substituent with an aryl moiety resulted in a significant improvement in antiparasitic activity (compound **3a** vs. **4a–c**) and resistance index. It was observed that the piperidine as a terminal ring in the carboxamide linker was favored over morpholine as a terminal ring (**3g** vs. **3d**). Furthermore, opening of the piperidine ring to *N*-diethylamine (**3g** vs. **3i**) resulted in a 13-fold decrease in antiparasitic activity. A halogen substitution on the quinoline ring led to an improvement in the antiparasitic activity. The third series of compounds bearing cyclic aminoalkyl carboxamide groups, that is, **5a–h**, were weakly active against *Plasmodium*, and the best analogue showed an IC₅₀ value of 28 μ m. The fourth series of compounds bearing benzylamino carboxamide groups, that is, **6a–c**, were found to be inactive with the lowest IC₅₀ value of 87 μ m. The final series bearing

anilino carboxamide groups, that is, **7a–c**, showed promising antiparasitic activity against all three *Plasmodium falciparum* strains. In this series, *para*-bromoanilino carboxamide **7b** displayed antiparasitic activity against the 3D7, Dd2, and Indo strains with IC₅₀ values of 2.1, 3.5, and 2 μ m, respectively, which were indicative of excellent resistance indices. Furthermore, **7b** showed good selectivity indices of 41 (HUH-7) and >48 (HEK-293T). On the basis of the in vitro antiparasitic activity and selectivity indices data presented in Table 1, compound **3g** was selected for further investigation.

Stage-specific kill kinetics of **3g** against erythrocytic stages of *P. falciparum*

To study the mechanistic properties of drug action, the in vitro stage-specific kill kinetics of **3g** were studied against the erythrocytic stages of *P. falciparum*. The synchronized Pf3D7 culture was treated with **3g** (IC₉₀ = 3.5 μ m) for different time points

Table 1. In vitro antiparasitodal activity, cytotoxicity against mammalian cells, and β -hematin inhibition potencies of C2-halo-C11 aliphatic aminoalkyl carboxamides **3a–n**, C2-aryl C11 aliphatic aminoalkyl carboxamides **4a–c**, C11 cyclic aminoalkyl carboxamides **5a–h**, C11 benzylamino carboxamides **6a–c**, and C11 anilino carboxamides **7a–c**.^[a]

Entry	Compound		<i>P. falciparum</i> IC ₅₀ [μ M]		Resistance index		Selectivity index		β -hematin inhib. IC ₅₀ [μ M]
	R ₁	R ₂	Pf3D7	PfDd2	PfAndo	PfDd2/Pf3D7	PfAndo/Pf3D7	HUH7/Pf3D7	
1	–	–	0.61 \pm 0.07	0.22 \pm 0.03	0.26 \pm 0.04	0.36	0.43	68.9	> 1000
3a	Br		9 \pm 1.1	22.8 \pm 3.0	9.8 \pm 1.3	2.5	1.1	5.8	nd
3b	F		> 100	nd	nd	nd	nd	nd	740 \pm 103
3c	F		> 100	nd	nd	nd	nd	nd	1000 \pm 110
3d	Br		> 100	nd	nd	nd	nd	nd	660 \pm 86
3e	H		> 100	nd	nd	nd	nd	nd	530 \pm 58
3f	Cl		4 \pm 0.5	9.4 \pm 1.1	8.2 \pm 1.1	2.4	2.1	> 25	395 \pm 55
3g	Br		1.3 \pm 0.2	6.3 \pm 0.8	5 \pm 0.7	4.8	3.8	46.9	840 \pm 76
3h	Br		36 \pm 4.7	68 \pm 9.5	25 \pm 3.5	1.9	0.7	> 2.8	> 1000
3i	Br		17.5 \pm 2.5	100 \pm 11.0	83 \pm 12.5	5.7	4.7	1.4	nd
3j	Cl		9 \pm 1.1	> 25	10.4 \pm 1.1	nd	1.2	3.3	1000 \pm 120
3k	Cl		17 \pm 2.1	16 \pm 2.1	< 12.5	0.94	nd	2.4	nd
3l	Cl		81 \pm 9.7	nd	nd	nd	nd	nd	960 \pm 140
3m	Br		43 \pm 5.6	nd	nd	nd	nd	nd	700 \pm 98
3n	F		42 \pm 5.9	30 \pm 3.6	28 \pm 3.4	0.7	0.7	1.4	> 1000
4a	<i>p</i> -F		2.7 \pm 0.3	10.8 \pm 1.1	7.8 \pm 1.0	4	2.9	> 37	930 \pm 74
4b	<i>p</i> -NHAc		4.7 \pm 0.6	8.2 \pm 1.2	3.4 \pm 0.4	1.7	0.7	18.3	580 \pm 41
4c	<i>p</i> -Ac		6.5 \pm 0.7	4.7 \pm 0.8	2.3 \pm 0.3	0.7	0.4	8.3	> 1000
5a	Cl		33 \pm 4.6	17 \pm 2.3	< 12.5	0.51	nd	> 3	500 \pm 60
5b	Cl		30 \pm 3.9	36 \pm 4.7	30 \pm 4.2	1.2	1	> 3.3	690 \pm 97
5c	Br		36 \pm 4.3	34 \pm 4.1	36 \pm 4.3	0.94	1	> 2.8	540 \pm 43

Table 1. (Continued)

Entry	Compound		<i>P. falciparum</i> IC ₅₀ [μM]			Resistance index	Selectivity index	β-hematin inhib. IC ₅₀ [μM]		
	R ₁	R ₂	<i>Pf</i> 3D7	<i>Pf</i> Dd2	<i>Pf</i> Ando	<i>Pf</i> Dd2/ <i>Pf</i> 3D7	<i>Pf</i> Ando/ <i>Pf</i> 3D7	HUH7/ <i>Pf</i> 3D7	HEK293T/ <i>Pf</i> 3D7	
5d	F		100 ± 14.0	nd	nd	nd	nd	nd	nd	860 ± 60
5e	H		> 100	nd	nd	nd	nd	nd	nd	740 ± 81
5f	H		> 100	nd	nd	nd	nd	nd	nd	660 ± 92
5g	Cl		45 ± 5.0	28 ± 3.9	28 ± 3.6	0.6	0.6	> 2.2	> 2.2	670 ± 40
5h	Cl		28 ± 3.4	23 ± 2.8	27 ± 3.0	0.8	0.97	> 3.5	> 3.5	930 ± 74
6a	Br	<i>p</i> -OCF ₃	> 100	nd	nd	nd	nd	nd	nd	820 ± 33
6b	Br	<i>p</i> -CF ₃	87 ± 12.2	nd	nd	nd	nd	nd	nd	745 ± 60
6c	Br	<i>m</i> -CF ₃	> 100	nd	nd	nd	nd	nd	nd	815 ± 49
7a	Br	<i>p</i> -OCF ₃	10.3 ± 0.9	38 ± 4.9	38 ± 5.3	3.7	3.7	9.2	> 9.7	> 1000
7b	Br	<i>p</i> -Br	2.1 ± 0.3	3.5 ± 0.4	2 ± 0.4	1.7	1	41	> 48	> 1000
7c	Br	<i>p</i> -F	10 ± 1.2	5 ± 0.6	5 ± 0.6	0.5	0.5	5	2.5	> 1000
	CQ-diphosphate		0.04 ± 0.003	0.168 ± 0.01	0.44 ± 0.05	4.2	11	> 200	> 200	1120 ± 134

[a] nd: not determined; resistance index = IC₅₀(resistant strain)/IC₅₀ (sensitive strain); selectivity index = CC₅₀(cytotoxicity)/IC₅₀ (antimalarial activity); IC₅₀ columns show mean ± standard deviation of two independent experiments taking three replicates for each experiment.

(rings: 12, 24, 36, and 48 h; trophozoites: 3, 6, 18, and 24 h; schizonts: 3, 6, and 12 h). After drug exposure, the drug pressure was withdrawn by centrifugal removal of conditioned medium followed by media wash. Further, the washed parasites were allowed to grow in drug-free media under normal culture conditions for a total period of 96 (rings), 72 (trophozoites), and 60 h (schizonts). After incubation, the growth of the parasites was measured by microscopic evaluation of Giemsa-stained smears (Figure 3). The results suggested that cryptolepine analogue **3g** actively inhibited the trophozoite-stage parasites (Figure 3B). Further, removal of **3g** by aspiration of conditioned medium followed by maintenance in drug-free medium failed to revive the parasites. This cytotoxic action of **3g** was observed as early as 3 h. The action of **3g** on ring-stage parasite was relatively slow, and it failed to show cytotoxic drug action until an exposure time of 48 h (Figure 3A). However, at earlier time points (12–36 h), rings treated with **3g** showed a significant (53–99%) decrease in parasitemia relative to the control. Although rings treated with **3g** matured into trophozoites, these trophozoites failed to progress further in the presence of the drug. However, the removal of **3g** from the ring-stage parasites treated with **3g** for 12–36 h allowed some of the parasites to revive from drug-caused stress, which was evident from increased parasitemia (1.5 to 12%) of the

drug-treated culture compared with initial parasitemia (1%) (Figure 3A). These results suggested possible cytostatic action (but not cytotoxic action) of short-term exposure of **3g** on ring-stage parasite. Treatment of schizonts with **3g** for 3 h followed by drug withdrawal resulted in a pronounced decrease in parasitemia, which suggested cytotoxic action of **3g** against schizonts. However, the killing was not complete, and approximately 3% parasitemia was observed at all time points of treatment. The relative percent parasitemia due to rings, trophozoites, and schizonts revealed an interesting phenomenon: a time-dependent effect with a greater number of schizonts in the 12 h treated parasites than in the 3 and 6 h treated parasites (Figure 3C).

Kinetics of **3g** uptake by malaria parasite

The intrinsic fluorescence of **3g** was used to study the uptake kinetics of **3g** by malaria parasite. As the kill kinetic studies indicated the trophozoites to be the most sensitive to the action of **3g**, the trophozoite-stage-enriched *Pf*3D7 culture was incubated with **3g** (50 μ M) at 37 °C for different time points. The washed cultures were observed under fluorescence (DAPI filter) and optical microscopy (Figure 4). At 15 min, diffuse, low-intensity fluorescence was observed in the entire cytosolic

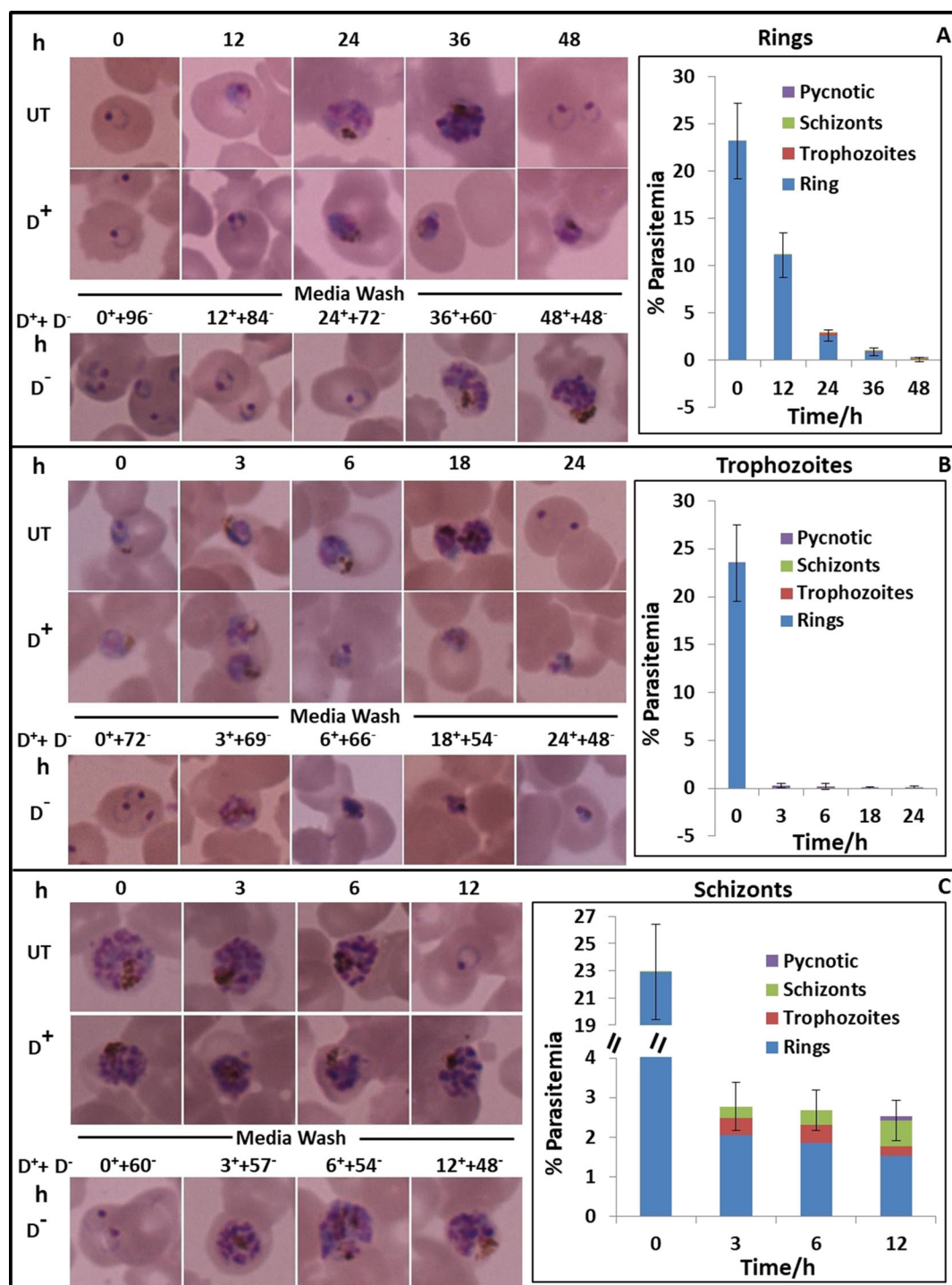


Figure 3. Stage-specific kill kinetics of **3g** against erythrocytic stages of *Pf3D7*. Synchronized ring (at 12, 24, 26, and 48 h), trophozoite (at 3, 6, 18, and 24 h), and schizont (at 3, 6, and 12 h) stage parasites were treated (D⁺) with the IC₅₀ value of **3g** (3.5 μM). In each case, **3g** was removed, and the culture was incubated in drug-free (D⁻) medium for a total period (D⁺ + D⁻) of 96 (ring), 72 (trophozoite), and 60 h (schizont). The effect of **3g** treatment was evaluated by Giemsa-stained blood smears under microscope. D⁺ represents drug pressure period and D⁻ represents drug-free period. The total parasitemia of each time point was calculated by analyzing microscopic images and was plotted in a bar diagram. Data shown in the histograms (panels A–C) represent mean ± standard deviation of three replicates.

region of infected red blood cells (RBCs). At 30 min, the fluorescence was found to be significantly concentrated and associated with the parasite. Continuous incubation of **3g** with parasite culture showed further reorganization of the stained parasite at 1 h. However, at 2 h, a dramatic increase in fluores-

cence intensity emanating from what appeared to be a densely stained entity was observed. The size of the fluorescent spot and its association with hemozoin suggested that **3g** may have targeted the food vacuole. Further, it was observed that between 3 and 6 h, the fluorescence intensity from the highly

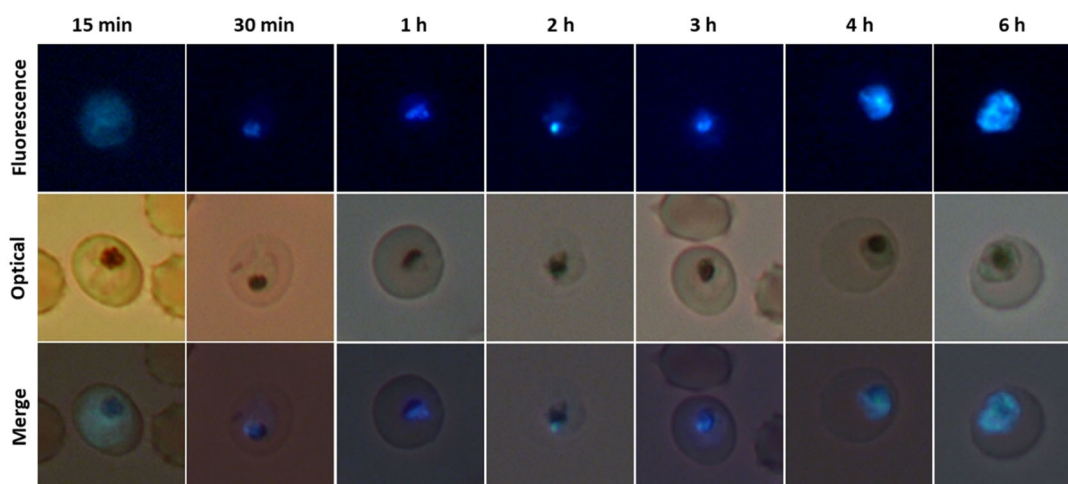


Figure 4. Kinetics of **3g** uptake by malaria parasite. Synchronized trophozoite culture ($\approx 4\%$ parasitemia and 2% hematocrit, $200\ \mu\text{L}$) was incubated with **3g** ($50\ \mu\text{M}$) at 37°C for the different time points indicated (15 min to 6 h). After each incubation, the culture was washed with $1\times$ PBS and was suspended again in PBS before observing the wet mount of each sample under fluorescence and optical microscopy. Drug accumulation was observed in close proximity to hemozoin crystals (seen as brown pigmented bodies in optical sections).

dense staining seen at 2 h began to spread out to a much larger area. In this context, it is worth noting that **3g**-mediated complete inhibition of trophozoite was also observed at 3 h (Figure 4). The temporal congruence of the staining characteristics and killing of the parasite suggested that kinetics and trafficking of **3g** were crucial to our mechanistic understanding of the action of **3g**.

Colocalization studies of **3g** fluorescence with EtBr and LysoTracker

Though cryptolepines are well known for their ability to intercalate with DNA,^[11] our observations suggested that **3g** may have targeted the food vacuole. To find the intracellular site of accumulation of **3g** in malaria parasite, we decided to study the colocalization of **3g** with both DNA and food vacuole markers. We used EtBr, a well-known DNA-binding stain that emits red fluorescence,^[19] and LysoTracker red, a fluorophore that accumulates in acidic cell organelles such as food vacuoles^[20] for our colocalization studies. After 3 h incubation of parasites with **3g** ($50\ \mu\text{M}$), the washed cells were incubated with EtBr stain and LysoTracker red in separate experiments for 30 min at 37°C , and the washed cells were observed under fluorescence and optical microscopy (Figure 5A,B). The ring and schizont stages failed to show colocalization of EtBr and **3g** (Figure 5A). The fluorescence of **3g** appeared as a blue crown near red EtBr-stained genomic DNA eclipsing the nucleus only partially. The colocalization of the dispersed hemozoin with **3g** suggested that it may have affinity for hemozoin. Had it gained entry into the nucleus, it ought to have given uniform stain with complete colocalization of the red and blue stains. On the other hand, complete colocalization of the blue fluorescence of **3g** with the red fluorescence of LysoTracker (Figure 5B) confirmed the accumulation of **3g** in the food vacuole, in which the digestion of host hemoglobin takes place. These results suggested that **3g** was targeted not to the nu-

cleus but to the food vacuole, at which it seemed to interact with hemozoin (Figure 5B).

It is well known that quinoline-based drugs actively inhibit erythrocytic-stage parasites at the trophozoite stage, which is the stage of maximum growth associated with extensive proteolysis of hemoglobin and the resulting accumulation of a high concentration of heme.^[21] In molecular terms, quinolines are known to interact with free heme, preventing its detoxification through the formation of hemozoin and resulting in death of malaria parasite.^[21] Our microscopic studies also indicated that **3g** was more active against the trophozoite stage, which indicated possible targets for **3g** in the trophozoite stage. Further, colocalization of **3g** with LysoTracker proved its accumulation in the parasite food vacuole. Compound **3g** could possibly target one or more of the following four biochemical pathways operational in the food vacuole: 1) hemoglobin uptake pathway; 2) hemoglobin digestion pathway; 3) heme detoxification pathway; 4) amino acid transport pathway. To find the target of **3g**, we checked the activity of **3g** against the β -hematin formation and hemoglobin uptake pathways.

Inhibition of detergent-mediated β -hematin formation by **3g**

The β -hematin formation method described by Sandlin et al.^[22] was used with minor modifications. The β -hematin formation inhibitory potency of all the compounds studied by us is shown in Tables 1. In this assay, **3g** with an IC_{50} value of $840\ \mu\text{M}$ was found to show greater potency than CQ ($\text{IC}_{50} = 1120\ \mu\text{M}$). This β -hematin inhibitory activity together with the antiparasitic activity of **3g** suggested that, like CQ, **3g** accumulated in the food vacuole (Figures 4 and 5), in which it may have complexed with free heme to prevent its detoxification through the formation of hemozoin.^[22]

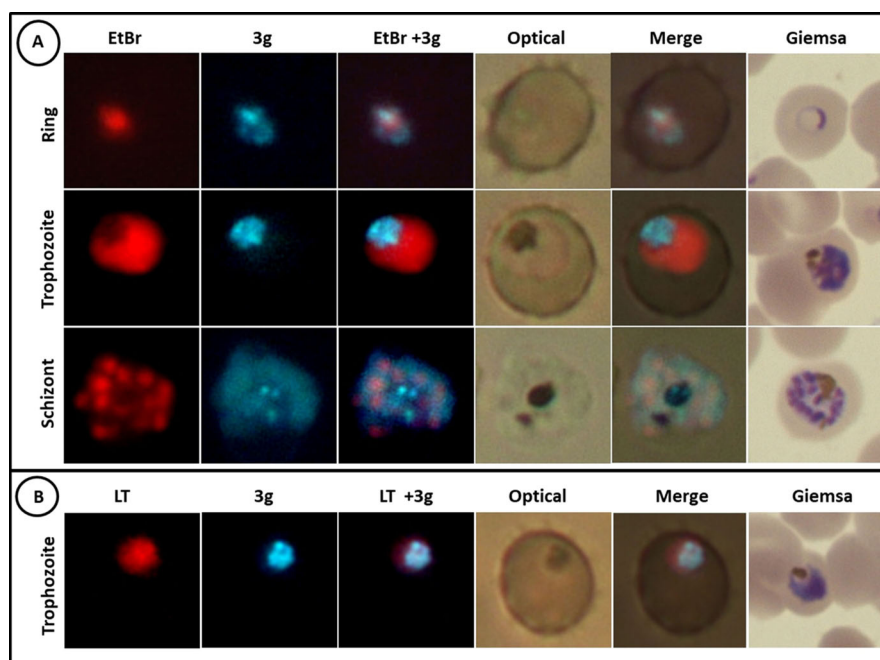


Figure 5. Colocalization of **3g** fluorescence with EtBr and LysoTracker (LT). The parasites were incubated with **3g** (50 μM) for 3 h. After incubation, the washed cultures were further incubated individually with EtBr and LysoTracker for 30 min. Then, the washed culture was observed under fluorescence microscopy as wet mount. A) EtBr and **3g** failed to show colocalization. B) The colocalization of LysoTracker and **3g** suggests the accumulation of **3g** in the food vacuole.

Indeed, similar to quinoline antimalarial drugs, the indoloquinoline “cryptolepine” has also been reported to form a ferriprotoporphyrin IX : cryptolepine complex $\{[\text{FP:C}]^+ m/z=848\}$ with FP.^[23] Therefore, we investigated whether non-quaternary cryptolepine derivative **3g** also formed a complex with heme. LC–MS analysis of a mixture containing 40 μM heme and 100 μM cryptolepine/**3g** in MeOH/H₂O (1:1, v/v; pH 7) indicated the formation of the respective monomer complexes $\{[\text{FP:C}]^+ m/z=848$ and $[\text{FP:3g}]^+ m/z=1066\}$ (Section S2, Supporting Information), which indicated the formation of the respective complexes with heme.

Although it is well known that cryptolepines may inhibit the growth of malaria parasite by inhibiting the formation of hemozoin, it is also true that derivatives of cryptolepines may have additional targets besides heme detoxification.^[10c] Hence, we examined if **3g** could also inhibit the endocytosis of hemoglobin by the food vacuole.

Inhibition of hemoglobin uptake by **3g**

Once we had confirmed the uptake and accumulation of **3g** in the food vacuole, we wanted to explore if **3g** could also inhibit the uptake of host hemoglobin and starve the parasite to death. Hence, we resorted to sorbitol-induced selective hemolysis^[24] to study the uptake of hemoglobin by the parasites and the inhibition of the same by **3g**. The principle of this method was based on the fact that the malaria parasite induces new permeation pathways (NPP) in the host red blood cell membrane that allow the entry of electroneutral and cationic solutes.^[25] These NPPs allow impermeable sorbitol into infected RBCs, which causes osmotic cell swelling and hemolysis.^[26] The

low permeability of uninfected and ring-stage-infected RBCs versus the high permeability of trophozoites and schizonts allows selective lysis of the latter, which allows quantitative estimation of the released hemoglobin by recording the absorbance at $\lambda=540\text{ nm}$ (A_{540}).^[25b] In the sorbitol-based assay, a molecule that inhibits hemoglobin uptake is expected to show a higher A_{540} value in the treated sample than in the untreated control. By comparing the A_{540} values by following the release of hemoglobin from an equal number of trophozoite-stage-infected RBCs at 0 and 15 h, we first calculated the A_{540} value representing the amount of hemoglobin taken up by untreated parasite (Figure 6A). To measure the effect of **3g** on hemoglobin uptake, synchronized trophozoite stage (28 h post-invasion) *P. falciparum* 3D7 cultures (4% parasitemia, 2% hematocrit) were treated with the IC₉₀ (3.5 μM) of **3g** for 15 h. The relative hemoglobin contents of the treated and untreated parasitized red blood cells (PRBCs) taken at identical numbers were determined in terms of A_{540} by following sorbitol-mediated hemolysis. As expected, sorbitol induced lysis from 15 h, and untreated culture showed less hemoglobin ($A_{540}\approx 0.28$) than the 0 h untreated parasite culture ($A_{540}\approx 0.6$) (Figure 6A). This decrease in hemoglobin amount to about half was due to voracious consumption of hemoglobin in the trophozoite stage. In contrast, we found a higher amount of hemoglobin ($A_{540}\approx 0.45$) in PRBCs treated with **3g** for 15 h as compared with untreated PRBCs ($A_{540}\approx 0.28$). This higher amount of hemoglobin release from **3g**-treated PRBCs suggested that **3g** inhibited the uptake of hemoglobin by parasite. Microscopic observations of untreated and **3g**-treated cultures at 0 and 15 h confirmed that the **3g**-treated parasites were inhibited at the trophozoite stage, whereas the untreated trophozoite stage

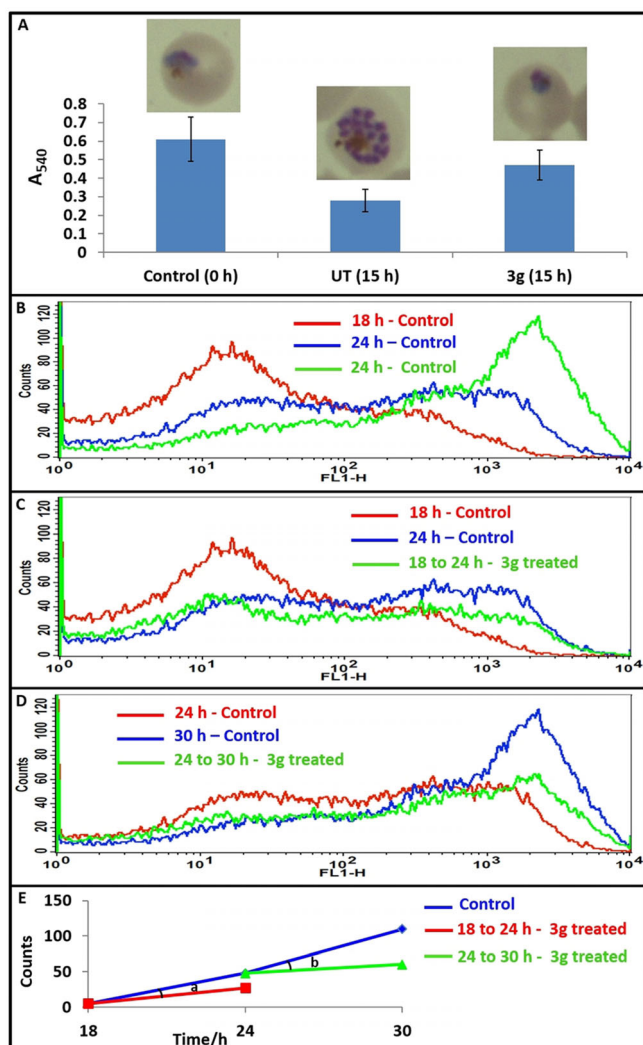


Figure 6. A) Inhibition of hemoglobin uptake by **3g**. The effect of hemoglobin uptake in the presence of **3g** was studied by the sorbitol-induced hemolysis method by using a spectrophotometer. Hemoglobin released was measured by absorbance at $\lambda = 540$ nm. The significantly higher amount of hemoglobin in the sample treated with **3g** for 15 h as compared with the corresponding untreated (UT) 15 h sample suggests inhibition of hemoglobin uptake by the malaria parasite. Data shown in the histograms represent mean \pm standard deviation of three independently done experiments taking two replicates for each experiment. B–E) FACS analysis of inhibition of FITC-dextran endocytosis by malaria parasite. The 18 and 24 h trophozoite-stage cultures, growing in FITC-dextran-resealed RBCs, were incubated without and with **3g** (at the IC_{90} value) for 6 h periods between a) 18–24 h and b) 24–30 h, respectively, following which the parasites were isolated by saponin hemolysis. Untreated control parasites at 18 h of growth and b) 24 h of growth as well as test parasites treated with **3g** for c) 18–24 h and d) 24–30 h were analyzed for the FITC signal by FACS taking 2000 parasites in each case. B) This panel shows a progressive increase in the intensity of FITC-dextran in 18, 24, and 30 h parasite cultures. C) This panel shows data for 18–24 h **3g**-treated sample in comparison with the 18 and 24 h untreated controls. D) This panel shows data for 24–30 h **3g**-treated sample in comparison with 24 and 30 h untreated controls. A decreased fluorescence signal in the treated samples is observed at both of these time points. E) This panel represents the cell counts at 2×10^3 signal intensity for the three controls (18, 24, and 30 h) and the two **3g**-treated (18–24 and 24–30 h) samples. Relative to untreated control (blue line), there is decreased uptake of FITC-dextran in the **3g**-treated sample at time points 24 h (red line) and 30 h (green line). The control shows a linear rise in uptake signal, whereas both the treated samples show significantly diminished uptake signals. The fact that angle b is approximately twofold larger than angle a indicates that inhibition of endocytosis is greater at 24–30 h than at 18–24 h.

transited to the schizont stage at 15 h (Figure 5A). Our data suggests that the retarded growth of **3g**-treated parasite is likely due to reduced endocytosis of hemoglobin.

FACS analysis of inhibition of FITC-dextran endocytosis by malaria parasite

Invasion of merozoites into fluorescein isothiocyanate (FITC)-dextran-loaded resealed RBCs enabled us to assess the inhibition of the endocytic machinery of **3g**-treated malaria parasite by using fluorescence-activated cell sorting (FACS). In such resealed RBCs, the parasite was expected to endocytose both hemoglobin and the fluorescent FITC-dextran and transfer them both to the food vacuole. The high-intensity fluorescence signal emitted by FITC-dextran can be detected by FACS and, thus, provides a quantitative estimation of both the intensity of the signal and the number of cells carrying the signal. The 18 h (late ring) and 24 h (early trophozoites) cultures were treated with the IC_{90} value of **3g** for 6 h, and then the treated and untreated parasites were isolated from the host RBCs by using saponin hemolysis. These two time points corresponded to phases of the parasite life cycle at which the parasite devoured less (at 18 h) and more (at 24 h) hemoglobin. The isolated parasites were further analyzed by FACS for their uptake of FITC-dextran (Figure 6B–E). As shown in Figure 6B, the untreated controls of 18–30 h parasites showed a gradual increase in the fluorescence intensity as a result of the continuous uptake of FITC-dextran from resealed RBCs. In contrast, as shown in Figure 6C, the sample treated with **3g** from 18 to 24 h and analyzed by FACS at 24 h had 1.7-fold fewer fluorescent cells than the 24 h untreated sample, which suggested inhibition of endocytosis by the parasite at the late ring stage. Figure 6D shows that in an analogous experiment done on a 24 h early trophozoite stage culture, the number of fluorescent cells in the 30 h untreated control was twofold higher than that in the 24 h untreated sample, which suggested continued endocytosis during the 24–30 h time window. However, relative to the number of fluorescent cells for the 30 h control, the number of fluorescent cells for the sample treated with **3g** for the 24–30 h duration was approximately twofold lower, which suggested that inhibition of endocytosis by **3g** continued until 30 h. Figure 6E displays the analysis of the FACS data at a fluorescence intensity of 2×10^3 for **3g**-treated samples and untreated controls and demonstrates the inhibitory effect of **3g** on the endocytosis process. The fact that angle b (24 h) is approximately twofold larger than angle a (18 h) indicates greater inhibition of endocytosis at 24–30 h than at 18–24 h.

Physicochemical properties, CYP P450 inhibition, Caco-2 permeability, and pharmacokinetics of **3g**

The solubility of **3g** was determined in water, phosphate-buffered saline (PBS), simulated gastric fluid (SGF), and simulated intestinal fluid (SIF). Compound **3g** displayed low solubility ($< 10 \mu\text{g mL}^{-1}$) in water, PBS and SIF, whereas it showed high solubility in SGF ($400 \mu\text{g mL}^{-1}$). Further, **3g** was tested for inhibition of five major CYP450 isoenzymes, namely, CYP3A4, CYP2D6,

CYP2C9, CYP2C19, and CYP1A2, at 10 μM , and 47, 91, 26, 12, and 56% inhibition, respectively, was observed. The results indicated that compound **3g** showed moderate or very low inhibition of the CYP3A4, CYP2C9, and CYP2C19 enzymes. However, it showed higher inhibition of CYP2D6. Further, the Caco-2 permeability of **3g** was also investigated. This assay was done in a bidirectional (i.e., A2B and B2A) mode. The A2B apparent permeability (P_{app}) value of **3g** ($6.0 \times 10^{-6} \text{ cm s}^{-1}$) showed that it had high permeability through the membrane. The B2A value ($11.0 \times 10^{-6} \text{ cm s}^{-1}$) was approximately twofold higher than the A2B value (efflux ratio = 1.8). As per FDA acceptance criteria, if the efflux ratio is more than 2, it should be considered as an efflux substrate. As the efflux ratio is 1.8, **3g** is not a substrate of efflux transporter pump. Hence, these results indicate that **3g** has good solubility in gastric pH with no CYP3A4 or efflux liability.

To check the plasma exposure of the compound in a mouse model, the pharmacokinetics of compound **3g** were studied in healthy BALB/c mice following a single 10 mg kg^{-1} dose administration orally (p.o.) and a 1.0 mg kg^{-1} dose administration intravenously (i.v.). Plasma samples were collected at appropriate time points between the range of 0 to 24 h and were analyzed by LC-MS/MS. Compound **3g** showed good plasma exposure ($C_{\text{max}} = 585$ and 963 ng mL^{-1}) by both p.o. and i.v. routes. Compound **3g** displayed good availability by i.v. ($C_{\text{max}} = 963 \text{ ng mL}^{-1}$) as compared with p.o. ($C_{\text{max}} = 585 \text{ ng mL}^{-1}$) in plasma. However, the increased half-life of orally administered **3g** ($t_{1/2\beta} = 3 \text{ h}$) as compared to i.v.-administered **3g** ($t_{1/2\beta} = 0.55 \text{ h}$) suggests that the oral route has its merits. Furthermore, the $\text{AUC}_{0-\infty}$ (area under the curve from $t = 0$ extrapolated to infinity) of **3g** by the oral route was found to be $1243 \text{ ng h mL}^{-1}$, with oral bioavailability (%F) of 23%. The maximum concentration of **3g** in the plasma was observed at 585 ng mL^{-1} ($1.29 \mu\text{M}$) for 10 mg kg^{-1} of p.o. administration, which is nearly equal to the in vitro antiparasitodal IC_{50} value ($1.3 \mu\text{M}$).

In vivo antimalarial activity of **3g** in a *P. berghei* infected mouse model of malaria

The curative antimalarial potency of cryptolepine derivative **3g** was evaluated in a *P. berghei* (ANKA) infected mouse model of malaria. In view of the good pharmacokinetic properties with oral administration, compound **3g** (50 mg kg^{-1} BW) with 2% (hydroxypropyl)methyl cellulose in a solution of 2% Tween 80 in saline as a vehicle was administered orally to infected mice for four consecutive days. Microscopic evaluation of the results indicated that mice treated with **3g** showed 27–35% suppression of parasitemia from day 7 to day 13. The suppression of parasitemia also resulted in increased life span of the treated mice (average survival time: 27.8 ± 5 days) as compared to untreated control (average survival time: 20.2 ± 2.3 days) (Figure 7). Given that cryptolepines are known for their toxic properties, increased life span of treated mice suggests that cryptolepine derivative **3g** possesses good antimalarial activity along with low cytotoxicity. As the pharmacokinetic analysis showed that the maximum availability (C_{max}) of **3g** in plasma

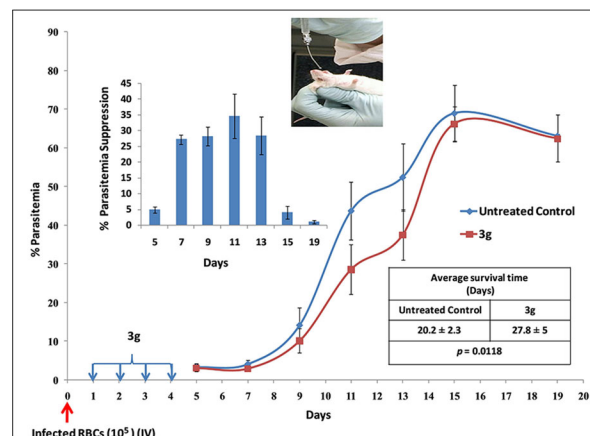


Figure 7. In vivo antimalarial efficacy of compound **3g** (50 mg kg^{-1} body weight, p.o.) in *P. berghei* infected BALB/c mice. The lines show mean percent parasitemia and standard deviation for five mice used/group of untreated (blue) and treated mice (red). Histogram shows the percent parasitemia suppression across days 5–19. Boxed data show the average survival time for untreated and treated mice. The p value (0.0118) of survival time calculated by using the student t-test (GraphPad Prism Software) indicates that there was a significant effect of **3g** on the longevity of treated mice.

for 10 mg kg^{-1} oral dose was 585 ng mL^{-1} or $1.3 \mu\text{M}$, which is equal to the in vitro anti *P. falciparum* IC_{50} value, we believe that the 50 mg kg^{-1} oral dose given in the in vivo mouse malaria experiment could have resulted in a substantially higher plasma concentration of **3g**. However, the inability of **3g** to show complete clearance of malaria parasite may be caused by different susceptibilities of *P. falciparum* 3D7 (a laboratory strain) and *P. berghei* ANKA (a mouse strain) and the possibility that the pharmacokinetics of the drugs are different in healthy and infected mice.

Conclusions

In summary, a new series of indolo[3,2-*b*]quinoline-C11-carboxamides were identified as promising orally bioavailable antimalarial agents. Aminoethylpiperidinylindolo[3,2-*b*]quinoline-C11-carboxamide **3g** displayed promising antiparasitodal activity ($\text{IC}_{50} = 1.3 \mu\text{M}$) against the CQ-sensitive Pf3D7 strain and also showed good antiparasitodal activities against the CQ-resistant Dd2 ($\text{IC}_{50} = 6.3 \mu\text{M}$) and Indo ($\text{IC}_{50} = 5.0 \mu\text{M}$) strains. Detailed mechanistic studies revealed that **3g** targeted the food vacuole of the parasite and inhibited the process of hemoglobin uptake. Antimalarial compound **3g** also showed acceptable oral pharmacokinetic properties and discernible in vivo antimalarial activity in *P. berghei* infected BALB/c mice. However, there is scope for molecular tweaking to improve its pharmacokinetics in infected animals. In summary, the present work demonstrated a proof of concept for the oral efficacy of C11 carboxamide non-quaternary cryptolepines in an animal model, opening new directions for future development of this class of compounds as novel antimalarial drugs. The fluorescent antimalarial compound **3g** could be effectively used as a probe for deeper understanding of its trafficking and mechanism of antimalarial action.

Experimental Section

General

All chemicals were obtained from Sigma–Aldrich Company and were used as received. ^1H , ^{13}C , and DEPT NMR spectra were recorded with Bruker Avance DPX FT-NMR 500 and 400 MHz instruments. Chemical data for ^1H NMR spectra are reported in parts per million (ppm) downfield from tetramethylsilane and are referenced to the residual proton in the NMR solvent (CD_3OD). ^{13}C NMR spectra were recorded at 125 or 100 MHz: chemical data for carbon atoms are reported in parts per million (ppm) downfield from tetramethylsilane and are referenced to the carbon resonance of the solvent (CD_3OD : $\delta=49.00$ ppm). ESI-MS and HRMS spectra were recorded with Agilent 1100 LC-Q-TOF and HRMS-6540-UHD machines. IR spectra were recorded with a PerkinElmer IR spectrophotometer. Melting points were recorded with a digital melting point apparatus. All compounds that were tested in biological assays were >95% pure. All animal experiments performed in the manuscript were conducted in compliance with institutional guidelines.

Synthesis

2-(2-Bromoacetamido)benzoic acid (9, RMS-101): A solution of anthranilic acid (**8**; 5.0 g, 36.4 mmol) in DMF and 1,4-dioxane (1:1, 30 mL) was cooled to 0 °C, and bromoacetyl bromide (4.0 mL, 45.8 mmol) was added dropwise over a 20 min period. The ice bath was then removed, and stirring was continued at room temperature for overnight. The mixture was added to water (150 mL), which resulted in the formation of a light-yellow precipitate. The precipitate was filtered and washed with an excess amount of water until neutral pH, and the solid residue was dried under vacuum to give compound **9** as a white solid (9.1 g, 96%): mp: 162–165 °C; ^1H NMR (400 MHz, CD_3OD): $\delta=8.46$ (d, $J=8.0$ Hz, 1 H), 8.00 (d, $J=8.0$ Hz, 1 H), 7.46 (t, $J=8.4$ Hz, 1 H), 7.07 (t, $J=8.4$ Hz, 1 H), 3.99 ppm (s, 2 H); MS (ESI): $m/z=256.9$ [$M+H$] $^+$.

2-[2-(Phenylamino)acetamido]benzoic acid (10, RMS-102): A solution of benzoic acid derivative **9** (5.0 g, 19.3 mmol) and aniline (6.3 mL, 69.4 mmol) in DMF (10 mL) was heated at 120 °C for 18 h. The mixture was then cooled to room temperature and poured into ice water (250 mL), and the pH was adjusted to 10–11 by using 5% KOH. Then, the mixture was extracted with dichloromethane (3 \times 100 mL), and combined dichloromethane layer was kept aside. The aqueous layer was acidified to pH 3 with a solution of 5% HBr, which resulted in the formation of a white precipitate. The precipitate was collected, washed with water, and dried to yield **10** as a white solid (3.66 g, 70%): mp: 194–197 °C; ^1H NMR (400 MHz, CD_3OD): $\delta=8.60$ (d, $J=8.0$ Hz, 1 H), 7.92 (d, $J=8.0$ Hz, 1 H), 7.43 (t, $J=8.8$ Hz, 1 H), 7.01 (t, $J=7.6$ Hz, 3 H), 6.54 (m, 3 H), 3.78 ppm (s, 2 H); MS (ESI): $m/z=270.0$ [$M+H$] $^+$.

Indolo[3,2-*b*]quinolin-11-one (11, RMS-103): A mixture of **10** (3.0 g, 21.5 mmol) and polyphosphoric acid (PPA, 200 g) was heated at 130 °C and stirred by using a mechanical stirrer for 2 h. The mixture was cooled to room temperature and poured into crushed ice (250 mL), neutralized with saturated KOH solution, and then extracted with EtOAc (2 \times 250 mL). The organic layer was washed with water and brine. The combined organic layer was dried with anhydrous Na_2SO_4 , and the solvent was evaporated under reduced pressure to give partially pure **11** as a light-brown solid (1.75 g, 67%): mp: >300 °C; ^1H NMR (400 MHz, $[\text{D}_6]\text{DMSO}$): $\delta=12.41$ (s, 1 H), 11.64 (s, 1 H), 8.29 (d, $J=7.9$ Hz, 1 H), 8.13 (d, $J=7.8$ Hz, 1 H), 7.72 (d, $J=7.4$ Hz, 1 H), 7.69 (dd, $J=7.4$, 12 Hz, 1 H), 7.51 (d, $J=8.4$ Hz, 1 H), 7.49 (dd, $J=7.7$, 12.4 Hz, 1 H), 7.29 (dd, $J=$

7.9, 12 Hz, 1 H), 7.20 ppm (dd, $J=7.7$, 12 Hz, 1 H); MS (ESI): $m/z=234.0$ [$M+H$] $^+$.

11-Chloro-10H-indolo[3,2-*b*]quinoline (12, RMS-104): A solution of **11** (1.5 g, 6.58 mmol) in POCl_3 (20 mL) was heated at reflux for 2 h. The mixture was cooled to room temperature and poured into crushed ice and neutralized with cold KOH solution. The product was extracted with EtOAc (3 \times 150 mL), and combined organic layer was dried with anhydrous Na_2SO_4 and concentrated under vacuum to give **12** (partially pure) as a light-brown solid (0.95 g, 60%): mp: 180–185 °C; ^1H NMR (400 MHz, $[\text{D}_6]\text{DMSO}$): $\delta=11.82$ (s, 1 H), 8.28 (d, $J=7.7$ Hz, 1 H), 8.21 (m, 2 H), 7.69 (m, 2 H), 7.61 (m, 2 H), 7.27 ppm (m, 1 H); MS (ESI): $m/z=253.0$ [$M+H$] $^+$.

10H-Indolo[3,2-*b*]quinoline (13, RMS-105): A solution of **12** (200 mg, 1 equiv), sodium acetate (1.0 g, 10 equiv), and 10% Pd/C in acetic acid (25 mL) was hydrogenated at 60 psi for 2 h by using a hydrogenation chamber. The mixture was filtered and washed with a small amount of AcOH, and acetic acid was evaporated and neutralized with ice-cold saturated NaHCO_3 solution. The product was extracted with EtOAc (3 \times 25 mL), and the combined organic layer was dried with anhydrous Na_2SO_4 . The solvent was evaporated under vacuum to give **13** as a yellow solid (180 mg, 80%): mp: 200–203 °C; ^1H NMR (400 MHz, $[\text{D}_6]\text{DMSO}$): $\delta=11.43$ (s, 1 H), 8.36 (d, $J=7.7$ Hz, 1 H), 8.29 (s, 1 H), 8.20 (d, $J=8.5$ Hz, 1 H), 8.11 (d, $J=8.1$ Hz, 1 H), 7.61 (m, 4 H), 7.29 ppm (dd, $J=7.0$, 12 Hz, 1 H); MS (ESI): $m/z=219.0$ [$M+H$] $^+$.^[10c]

Cryptolepine (1): Methyl iodide (3 equiv) was added to a stirred solution of indolo[3,2-*b*]quinoline **13** (500 mg, 1 equiv) in DMF (5 mL), and the mixture was heated at reflux at 100 °C for 6–8 h. The mixture was then cooled to room temperature, and EtOAc (10 mL) was added, which resulted in the formation of an orange-red solid. The solid was filtered, washed with an excess amount of EtOAc, and dried under vacuum to give cryptolepine (**1**, 70%): ^1H NMR (400 MHz, $[\text{D}_6]\text{DMSO}$): $\delta=12.89$ (s, 1 H), 9.29 (s, 1 H), 8.79 (dd, $J=8.4$, 13.6 Hz, 2 H), 8.59 (d, $J=8.0$ Hz, 1 H), 8.16 (t, $J=7.6$ Hz, 1 H), 7.94 (dd, $J=7.6$, 12.0 Hz, 2 H), 7.84 (d, $J=8.4$ Hz, 1 H), 7.51 (t, $J=7.6$ Hz, 1 H), 5.03 ppm (s, 3 H); ^{13}C NMR (100 MHz, $[\text{D}_6]\text{DMSO}$): $\delta=145.6$, 138.0, 135.2, 133.9, 133.2, 132.4, 129.8, 127.0, 126.2, 126.1, 124.7, 121.3, 117.8, 113.8, 113.1, 54.4 ppm; IR (CHCl_3): $\tilde{\nu}_{\text{max}}=3742$, 3435, 2920, 2850, 1637, 1609, 1577, 1503, 1452, 1384, 1252, 1034 cm^{-1} ; MS (ESI): $m/z=233.0$ [M] $^+$; HRMS: m/z calcd for $\text{C}_{16}\text{H}_{13}\text{N}_2$: 233.1073; found: 233.1071.^[17b]

2-[(Carboxymethyl)amino]benzoic acid (14, RMS-120): Sodium carbonate (200 g, 18.8 mmol) was added to a stirred solution of chloroacetic acid (347 g, 3.67 mol) in water (500 mL) at room temperature. The solution was then heated at 40–50 °C and was quickly added to a mixture of anthranilic acid (**8**; 500 g, 3.65 mmol) in water (340 mL) and 35% aq NaOH solution (320 mL). The resulting mixture was then heated at 40–45 °C for 4 days, and the solid mixture was treated with a solution of NaOH (150 g, 3.75 mmol) in water (4 L). The mixture was heated at 60 °C and filtered while hot. The solid residue was washed with 20% aq NaOH until the residue was dissolved. The combined filtrate was acidified with 37% aq HCl to pH 3, and the resulting precipitate was then filtered off and dried at 100 °C to yield **14** as a cream-colored solid (567 g, 80%): mp: 220 °C; ^1H NMR (400 MHz, CD_3OD): $\delta=8.30$ (d, $J=8.4$ Hz, 1 H), 7.70 (s, 1 H), 7.42 (d, $J=7.6$ Hz, 1 H), 7.28–7.17 (m, 2 H), 3.20 ppm (s, 2 H); MS (ESI): $m/z=195.0$ [$M+H$] $^+$.

2-[N-(Carboxymethyl)acetamido]benzoic acid (15, RMS-123): (Carboxymethylamino)benzoic acid (**14**; 10.0 g, 0.84 mmol) was added in small portions to a stirred solution of Na_2CO_3 (8.9 g, 0.84 mmol) in water (83.0 mL) at room temperature. Acetic anhy-

dride (8.56 0.84 mmol) was then added at room temperature with stirring. The mixture was stirred for 30 min and 37% aq HCl (14.0 mL) was added dropwise, which resulted in the formation of a precipitate. The solid product was filtered after 12 h, washed with water (3×15 mL), and air dried to give **15** as a light-brown solid (11.0 g): mp: 208–210 °C; ¹H NMR (400 MHz, CD₃OD): δ = 7.97 (d, *J* = 8.4 Hz, 1H), 7.56 (m, 2H), 7.44 (m, 1H), 3.60 (d, *J* = 8.4, 17.6 Hz, 2H), 1.69 ppm (s, 3H); MS (ESI): *m/z* = 260.0 [*M* + Na]⁺.

1-Acetyl-1*H*-indol-3-yl acetate (16, RMS-124): 2-[*N*-(Carboxymethyl)acetamido]benzoic acid (**15**; 1.36 g, 0.48 mmol) was added to a stirred solution of Ac₂O (4.6 g, 4.5 mmol) and triethylamine (1.3 g, 1.4 mmol). The mixture was heated at reflux for 20 min and concentrated under vacuum to give an oily residue (35 mL), which was refrigerated overnight. The solid product was filtered off and dried under vacuum to give product **16** as a light-green solid (80%): mp: 72–74 °C; ¹H NMR (400 MHz, CDCl₃): δ = 8.36 (d, *J* = 7.9 Hz, 1H), 7.90 (s, 1H), 7.41 (m, 3H), 2.62 (s, 3H), 2.39 ppm (s, 3H); MS (ESI): *m/z* = 217.0 [*M* + H]⁺.

General procedure for synthesis of 10*H*-indolo[3,2-*b*]quinoline-11-carboxylic acids 18a–d: A solution of 1-acetyl-1*H*-indol-3-yl acetate (**16**; 6.1 g, 0.23 mmol) in water (50 mL) was stirred for 30 min. A solution of isatin **17** (0.23 mmol) and KOH (26 g, 0.46 mmol) in water (50 mL) was added slowly. The mixture was heated at reflux for 4 h and was then cooled to 70 °C. Air was bubbled through the mixture for 20 min. The mixture was filtered, and the resulting filtrate was acidified to pH 1 with concd HCl. The precipitate was collected and washed with water and dried under vacuum to give carboxylic acid **18**, which was used in the next step without further purification.

10*H*-Indolo[3,2-*b*]quinoline-11-carboxylic acid (18a, RMS-125b): Light-green solid; mp: > 300 °C; ¹H NMR (400 MHz, [D₆]DMSO): δ = 11.52 (s, 1H), 9.38 (s, 1H), 8.37 (dd, *J* = 8.0, 17.4 Hz, 2H), 8.23 (d, *J* = 8.8 Hz, 1H), 7.84–7.78 (m, 2H), 7.69 (t, *J* = 7.6 Hz, 1H), 7.36 ppm (m, 2H); MS (ESI): *m/z* = 262.0 [*M* + H]⁺.

2-Bromo-10*H*-indolo[3,2-*b*]quinoline-11-carboxylic acid (18b, RMS-125a): Brown-red solid; mp: > 300 °C; ¹H NMR (400 MHz, [D₆]DMSO): δ = 11.54 (s, 1H), 9.40 (s, 2H), 8.39 (d, *J* = 7.6 Hz, 1H), 8.25 (d, *J* = 8.9 Hz, 1H), 7.86–7.69 (m, 3H), 7.40 ppm (t, *J* = 7.8 Hz, 1H); IR (CHCl₃): $\tilde{\nu}_{\text{max}}$ = 3670, 3645, 3584, 3418, 2921, 2348, 2054, 1612, 1460, 1317, 1122, 1048 cm^{−1}; MS (ESI): *m/z* = 341.2 [*M* + H]⁺.

2-Fluoro-10*H*-indolo[3,2-*b*]quinoline-11-carboxylic acid (18c, RMS-170): Brown-red solid; mp: > 300 °C; ¹H NMR (400 MHz, [D₆]DMSO): δ = 11.50 (s, 1H), 8.90 (d, *J* = 10 Hz, 1H), 8.34 (m, 2H), 7.80 (d, *J* = 8.8 Hz, 1H), 7.69–7.61 (m, 2H), 7.35 ppm (t, *J* = 7.6 Hz, 1H); MS (ESI): *m/z* = 280.0 [*M* + H]⁺.

2-Chloro-10*H*-indolo[3,2-*b*]quinoline-11-carboxylic acid (18d, RMS-187): Dark-green solid; mp: 310–312 °C; ¹H NMR (400 MHz, [D₆]DMSO): δ = 11.52 (s, 1H), 9.22 (s, 1H), 8.37 (d, *J* = 7.6 Hz, 1H), 8.30 (d, *J* = 9.2 Hz, 1H), 7.80 (d, *J* = 8.4 Hz, 1H), 7.74–7.66 (m, 2H), 7.36 ppm (t, *J* = 7.2 Hz, 1H); MS (ESI): *m/z* = 296.0 [*M* + H]⁺.

General procedure for synthesis of 10*H*-indolo[3,2-*b*]quinoline-C11-carboxamides 3a–n, 5a–h, 6a–c, and 7a–c: HBTU (1.2 equiv) and diisopropylethylamine (3 equiv) were added to a stirred solution of 10*H*-indolo[3,2-*b*]quinoline-C11-carboxylic acid **18** (300 mg, 1 equiv) in anhydrous DMF (10 mL) under a N₂ atmosphere at room temperature. After stirring for 10 min, alkylamine **19**, **21**, or **22** (1.1 equiv) was added to the stirring solution. The mixture was stirred for another 24 h, and then ice-cold water was added. The product was extracted with ethyl acetate (3×50 mL), and the obtained organic layer was dried with anhydrous Na₂SO₄. The solvent

was evaporated under reduced pressure, and the obtained crude product was purified by silica gel (#100–200) column chromatography (5–10% MeOH/CH₂Cl₂) to give C11-carboxamide **3a–n**, **5a–h**, **6a–c**, or **7a–c** (40–60%).

2-Bromo-*N*-(3-morpholinopropyl)-10*H*-indolo[3,2-*b*]quinoline-11-carboxamide (3a, RMS-126): Yellow amorphous solid; mp: 247–249 °C; ¹H NMR (400 MHz, CD₃OD): δ = 8.36 (d, *J* = 7.6 Hz, 1H), 8.24 (d, *J* = 2.0 Hz, 1H), 8.06 (d, *J* = 8.8 Hz, 1H), 7.70 (dd, *J* = 9.2, 2.0 Hz, 1H), 7.57 (t, *J* = 7.6 Hz, 1H), 7.49 (d, *J* = 8.4 Hz, 1H), 7.25 (t, *J* = 7.2 Hz, 1H), 3.60 (m, 4H), 3.20 (m, 4H), 2.64 (m, 4H), 1.93 ppm (m, 2H); ¹³C NMR (100 MHz, [D₆]DMSO): δ = 164.4, 146.8, 144.6, 141.5, 131.3, 130.5, 129.0, 126.1, 123.8, 121.4, 120.4, 120.0, 119.6, 118.7, 111.9, 66.1, 56.0, 53.3, 37.8, 25.6 ppm; IR (CHCl₃): $\tilde{\nu}_{\text{max}}$ = 3436, 2065, 1632, 1465, 1019 cm^{−1}; MS (ESI): *m/z* = 468.9 [*M* + H]⁺; HRMS: *m/z* calcd for C₂₃H₂₂BrN₄O₂ + H⁺: 467.1077; found: 467.1066; HPLC: *t*_R = 16.02 min, purity: 95.8%.

2-Fluoro-*N*-(3-morpholinopropyl)-10*H*-indolo[3,2-*b*]quinoline-11-carboxamide (3b, RMS-172): Yellow amorphous solid; mp: 274–275 °C; ¹H NMR (400 MHz, [D₆]DMSO): δ = 11.39 (s, 1H), 8.91 (t, *J* = 5.2 Hz, 1H), 8.26 (m, 2H), 7.71 (d, *J* = 10.8 Hz, 1H), 7.57 (m, 3H), 7.25 (t, *J* = 6.8 Hz, 1H), 3.30 (m, 6H), 3.23 (m, 2H), 2.37 (m, 4H), 1.76 ppm (m, 2H); ¹³C NMR (100 MHz, [D₆]DMSO): δ = 164.5, 160.3 (d, ¹*J*_{CF} = 242.0 Hz), 146.1, 144.3, 140.2, 131.8, 130.2, 129.1, 123.3, 123.2, 121.2, 120.5, 119.9, 116.3 (d, ²*J*_{CF} = 23.8 Hz), 111.9, 107.4 (d, ²*J*_{CF} = 23.5 Hz), 66.1, 56.0, 53.3, 37.8, 25.6 ppm; IR (CHCl₃): $\tilde{\nu}_{\text{max}}$ = 3406, 2918, 2849, 2343, 1649, 1454, 1022 cm^{−1}; MS (ESI): *m/z* = 407.2 [*M* + H]⁺, HRMS: *m/z* calcd for C₂₃H₂₃FN₄O₂ + H⁺: 407.1878; found: 407.1880; HPLC: *t*_R = 35.33 min, purity: 99.5%.

2-Fluoro-*N*-(2-morpholinoethyl)-10*H*-indolo[3,2-*b*]quinoline-11-carboxamide (3c, RMS-171): Yellow amorphous solid; mp: 219–221 °C; ¹H NMR (400 MHz, [D₆]DMSO): δ = 11.50 (s, 1H), 8.96 (s, 1H), 8.39 (m, 2H), 8.23 (d, *J* = 9.6 Hz, 1H), 7.70 (m, 2H), 7.38 (t, *J* = 8.0 Hz, 1H), 4.12 (s, 4H), 3.75 (s, 2H), 2.69 (m, 2H), 2.61 ppm (m, 4H); ¹³C NMR (100 MHz, [D₆]DMSO): δ = 164.6, 160.7 (d, *J* = 241.8 Hz), 146.0, 144.2, 140.3, 131.8, 130.1, 129.3, 123.4, 121.1, 120.5, 119.9, 116.4 (d, *J* = 26.2 Hz), 111.9, 108.0 (d, *J* = 23.4 Hz), 66.0, 57.0, 53.1, 35.9 ppm; IR (CHCl₃): $\tilde{\nu}_{\text{max}}$ = 3401, 2918, 2850, 1741, 1632, 1576, 1539, 1512, 1492, 1463, 1400, 1333, 1214, 1194, 1116, 1148, 1079, 1021 cm^{−1}; MS (ESI): *m/z* = 393.1 [*M* + H]⁺; HRMS: *m/z* calcd for C₂₂H₂₁FN₄O₂ + H⁺: 393.1721; found: 393.1748; HPLC: *t*_R = 29.94 min, purity: 95.3%.

2-Bromo-*N*-(2-morpholinoethyl)-10*H*-indolo[3,2-*b*]quinoline-11-carboxamide (3d, RMS-138): Yellow amorphous solid; mp: 250–252 °C; ¹H NMR (400 MHz, CD₃OD): δ = 8.53 (s, 1H), 8.51 (d, *J* = 7.6 Hz, 1H), 8.20 (d, *J* = 9.2 Hz, 1H), 7.93 (s, 1H), 7.85 (d, *J* = 9.2 Hz, 1H), 7.71 (t, *J* = 8.0 Hz, 1H), 7.63 (d, *J* = 8.0 Hz, 1H), 7.39 (t, *J* = 7.2 Hz, 1H), 3.85 (m, 6H), 2.81 ppm (m, 6H); ¹³C NMR (100 MHz, [D₆]DMSO): δ = 164.4, 146.7, 144.5, 141.6, 131.2, 130.5, 129.18, 129.12, 126.4, 123.9, 121.4, 120.4, 120.0, 119.7, 118.7, 111.9, 66.2, 57.3, 53.2, 36.0 ppm; IR (CHCl₃): $\tilde{\nu}_{\text{max}}$ = 3437, 2922, 1617, 1380, 1033, 1019 cm^{−1}; MS (ESI): *m/z* = 452.8 [*M* + H]⁺; HRMS: *m/z* calcd for C₂₂H₂₁BrN₄O₂ + H⁺: 453.0921; found: 453.0907; HPLC: *t*_R = 8.4 min, purity: 97.7%.

***N*-(2-Morpholinoethyl)-10*H*-indolo[3,2-*b*]quinoline-11-carboxamide (3e, RMS-173):** Yellow amorphous solid; mp: 240–241 °C; ¹H NMR (400 MHz, [D₆]DMSO): δ = 11.27 (s, 1H), 8.80 (t, *J* = 5.6 Hz, 1H), 8.29 (m, 2H), 8.18 (d, *J* = 8.4 Hz, 1H), 7.65–7.52 (m, 4H), 7.24 (t, *J* = 8.0 Hz, 1H), 3.61 (m, 2H), 3.24 (m, 4H), 2.58 (m, 2H), 2.47 ppm (m, 4H); ¹³C NMR (100 MHz, [D₆]DMSO): δ = 164.9, 146.1, 144.2, 143.1, 130.0, 129.0, 128.7, 126.1, 125.5, 124.8, 122.7, 121.3, 120.8, 120.6, 119.7, 111.7, 66.2, 57.0, 53.1, 36.1 ppm; IR (CHCl₃):

$\tilde{\nu}_{\max}$ = 3401, 2920, 2851, 1741, 1643, 1461, 1491, 1461, 1336, 1115, 1021 cm^{-1} ; MS (ESI): m/z = 375.0 $[M+H]^+$; HRMS: m/z calcd for $\text{C}_{22}\text{H}_{22}\text{N}_4\text{O}_2 + \text{H}^+$: 375.1816; found: 375.1820; HPLC: t_R = 4.62 min, purity: 100%.

2-Chloro-*N*-[2-(pyrrolidin-1-yl)ethyl]-10*H*-indolo[3,2-*b*]quinoline-11-carboxamide (3f, RMS-200): Yellow amorphous solid; mp: 250–251 °C; ^1H NMR (400 MHz, $[\text{D}_6]\text{DMSO}$): δ = 11.59 (s, 1H), 9.08 (s, 1H), 8.38 (d, J = 7.6 Hz, 1H), 8.28 (d, J = 8.8 Hz, 2H), 7.72 (m, 2H), 7.63 (d, J = 8.0 Hz, 1H), 7.34 (t, J = 7.2 Hz, 1H), 3.72 (m, 2H), 3.43 (m, 6H, merged with $[\text{D}_6]\text{DMSO}$ signal), 1.91 ppm (m, 4H); ^{13}C NMR (125 MHz, $[\text{D}_6]\text{DMSO}$): δ = 164.7, 146.7, 144.4, 141.4, 131.1, 130.6, 130.2, 129.4, 126.6, 123.2, 121.5, 120.4, 120.1, 111.8, 53.4, 22.9 ppm; IR (CHCl₃): $\tilde{\nu}_{\max}$ = 3417, 2921, 2852, 1743, 1621, 1540, 1463, 1384, 1214, 1021 cm^{-1} ; MS (ESI): m/z = 393.3 $[M+H]^+$; HRMS: m/z calcd for $\text{C}_{22}\text{H}_{21}\text{ClN}_4\text{O} + \text{H}^+$: 393.1477; found: 393.1494; HPLC: t_R = 8.78 min, purity: 98.6%.

2-Bromo-*N*-[2-(piperidin-1-yl)ethyl]-10*H*-indolo[3,2-*b*]quinoline-11-carboxamide (3g, RMS-148): Yellow amorphous solid; mp: 259–261 °C; ^1H NMR (400 MHz, CD_3OD): δ = 10.14 (s, 1H), 8.36 (d, J = 8.0 Hz, 1H), 8.32 (s, 1H), 8.07 (d, J = 8.8 Hz, 1H), 7.65 (d, J = 8.8 Hz, 1H), 7.58 (t, J = 7.6 Hz, 1H), 7.32 (t, J = 7.2 Hz, 2H), 7.27 (m, 1H), 3.91 (m, 2H), 2.82 (m, 2H), 2.68 (m, 4H), 1.68 (m, 4H), 1.52 ppm (m, 2H); ^{13}C NMR (100 MHz, $[\text{D}_6]\text{DMSO}$): δ = 164.3, 146.7, 144.4, 141.6, 131.2, 130.5, 129.2, 129.1, 126.4, 123.9, 121.4, 120.5, 120.0, 119.6, 118.7, 111.8, 57.43, 54.8, 53.9, 36.4, 25.4, 23.9 ppm; IR (CHCl₃): $\tilde{\nu}_{\max}$ = 3439, 2959, 2925, 2852, 2096, 1930, 1640, 1596, 1575, 1491, 1454, 1436, 1407, 1389, 1367, 1294, 1192, 1175, 1158, 1129, 1083, 1046, 1023 cm^{-1} ; MS (ESI): m/z = 452.9 $[M+H]^+$; HRMS: m/z calcd for $\text{C}_{23}\text{H}_{23}\text{BrN}_4\text{O} + \text{H}^+$: 451.1128; found: 451.1124; HPLC: t_R = 24.53 min, purity: 97.9%.

2-Bromo-*N*-(3-hydroxypropyl)-10*H*-indolo[3,2-*b*]quinoline-11-carboxamide (3h, RMS-149): Yellow amorphous solid; mp: 277–278 °C; ^1H NMR (400 MHz, CD_3OD): δ = 11.12 (brs, 1H), 8.30 (d, J = 8.0 Hz, 1H), 8.20 (s, 1H), 7.98 (d, J = 9.2 Hz, 1H), 7.79 (s, 1H), 7.63 (d, J = 8.8 Hz, 1H), 7.53 (t, J = 8.0 Hz, 1H), 7.44 (d, J = 8.0 Hz, 1H), 7.21 (t, J = 7.6 Hz, 1H), 3.72 (t, J = 6.0 Hz, 2H), 3.64 (t, J = 6.8 Hz, 2H), 1.93 ppm (m, 2H); ^{13}C NMR (100 MHz, CD_3OD): δ = 167.6, 148.5, 146.3, 142.9, 132.0, 131.23, 131.18, 130.9, 127.5, 125.4, 122.9, 121.65, 121.6, 120.9, 120.7, 112.8, 61.1, 38.8, 32.9 ppm; IR (CHCl₃): $\tilde{\nu}_{\max}$ = 3493, 2919, 2850, 1730, 1649, 1465, 1286, 1072 cm^{-1} ; MS (ESI): m/z = 398.0 $[M+H]^+$; HRMS: m/z calcd for $\text{C}_{19}\text{H}_{16}\text{BrN}_3\text{O}_2 + \text{H}^+$: 398.0499; found: 398.0512; HPLC: t_R = 27.45 min, purity: 94.9%.

2-Bromo-*N*-[2-(diethylamino)ethyl]-10*H*-indolo[3,2-*b*]quinoline-11-carboxamide (3i, RMS-127): Yellow amorphous solid; mp: 203–205 °C; ^1H NMR (400 MHz, CD_3OD): δ = 8.45 (d, J = 8.0 Hz, 1H), 8.42 (s, 1H), 8.14 (d, J = 8.8 Hz, 1H), 7.79 (d, J = 9.2 Hz, 1H), 7.67 (t, J = 8.0 Hz, 1H), 7.58 (d, J = 8.0 Hz, 1H), 7.34 (t, J = 7.2 Hz, 1H), 3.84 (t, J = 6.4 Hz, 2H), 3.15 (s, 2H), 3.06 (m, 4H), 1.36–1.26 ppm (m, 6H); ^{13}C NMR (100 MHz, $\text{CDCl}_3 + \text{CD}_3\text{OD}$): δ = 168.1, 148.5, 146.0, 143.1, 132.3, 132.0, 131.3, 130.1, 127.7, 125.5, 123.4, 121.9, 121.5, 119.6, 112.8, 52.4, 48.3, 38.1, 11.2 ppm; IR (CHCl₃): $\tilde{\nu}_{\max}$ = 3436, 2070, 1633, 1464, 1157, 1019 cm^{-1} ; MS (ESI): m/z = 439.0 $[M+H]^+$; HRMS: m/z calcd for $\text{C}_{22}\text{H}_{23}\text{BrN}_4\text{O} + \text{H}^+$: 439.1128; found: 439.1116; HPLC: t_R = 45.10 min, purity: 95.4%.

2-Chloro-*N*-[2-(dimethylamino)ethyl]-10*H*-indolo[3,2-*b*]quinoline-11-carboxamide (3j, RMS-201): Yellow amorphous solid; mp: 231–233 °C; ^1H NMR (400 MHz, $[\text{D}_6]\text{DMSO}$): δ = 8.99 (s, 1H), 8.38–8.25 (m, 3H), 7.71–7.61 (m, 3H), 7.34 (m, 1H), 3.45 (m, 2H), 2.75 (m, 2H), 2.47 ppm (s, 6H); ^{13}C NMR (125 MHz, $[\text{D}_6]\text{DMSO}$): δ = 164.6, 146.7, 144.4, 141.4, 131.0, 130.5, 130.2, 129.7, 126.6, 123.3, 123.2, 121.5, 120.5, 120.1, 119.3, 111.8, 57.1, 44.3, 36.5 ppm; IR (CHCl₃):

$\tilde{\nu}_{\max}$ = 3401, 2920, 2851, 1627, 1487, 1462, 1336, 1212, 1193, 1022 cm^{-1} ; MS (ESI): m/z = 367.3 $[M+H]^+$; HRMS: m/z calcd for $\text{C}_{20}\text{H}_{19}\text{ClN}_4\text{O} + \text{H}^+$: 367.1320; found: 367.1343; HPLC: t_R = 4.87 min, purity: 100%.

2-Chloro-*N*-[3-(dimethylamino)propyl]-10*H*-indolo[3,2-*b*]quinoline-11-carboxamide (3k, RMS-202): Yellow amorphous solid; mp: 216–218 °C; ^1H NMR (400 MHz, $[\text{D}_6]\text{DMSO}$): δ = 11.56 (s, 1H), 9.11 (s, 1H), 8.38 (d, J = 8.0 Hz, 1H), 8.29 (d, J = 9.2 Hz, 1H), 8.13 (s, 1H), 7.73–7.63 (m, 3H), 7.35 (t, J = 7.2 Hz, 1H), 3.20 (m, 2H), 2.83 (s, 6H), 2.55 (m, 2H), 2.05 ppm (m, 2H); ^{13}C NMR (125 MHz, $[\text{D}_6]\text{DMSO}$): δ = 164.7, 146.8, 144.5, 141.3, 131.2, 130.6, 130.2, 129.1, 126.6, 123.2, 122.8, 121.5, 120.5, 120.2, 119.1, 111.9, 54.9, 42.4, 36.6, 24.1 ppm; IR (CHCl₃): $\tilde{\nu}_{\max}$ = 3401, 2920, 2850, 1741, 1619, 1541, 1463, 1384, 1021 cm^{-1} ; MS (ESI): m/z = 381.3 $[M+H]^+$; HRMS: m/z calcd for $\text{C}_{21}\text{H}_{21}\text{ClN}_4\text{O} + \text{H}^+$: 381.1477; found: 381.1500; HPLC: t_R = 4.87 min, purity: 100%.

2-Chloro-*N*-[3-(diethylamino)propyl]-10*H*-indolo[3,2-*b*]quinoline-11-carboxamide (3l, RMS-203): Yellow amorphous solid; mp: 218–222 °C; ^1H NMR (400 MHz, $[\text{D}_6]\text{DMSO}$): δ = 11.58 (s, 1H), 9.12 (s, 1H), 8.28 (d, J = 8.0 Hz, 1H), 8.29 (d, J = 8.8 Hz, 1H), 8.13 (s, 1H), 7.74–7.62 (m, 3H), 7.35 (t, J = 7.6 Hz, 1H), 3.39 (m, 2H, merged with $[\text{D}_6]\text{DMSO}$), 3.17 (m, 6H), 2.02 (m, 2H), 1.21 ppm (t, J = 7.2 Hz, 6H); ^{13}C NMR (125 MHz, $[\text{D}_6]\text{DMSO}$): δ = 164.7, 146.9, 144.5, 141.4, 131.2, 130.6, 130.2, 129.1, 126.6, 123.2, 122.7, 121.5, 120.4, 120.2, 119.2, 111.9, 48.8, 46.6, 36.7, 23.4, 8.6 ppm; IR (CHCl₃): $\tilde{\nu}_{\max}$ = 3411, 2920, 2851, 1741, 1618, 1577, 1455, 1384, 1021 cm^{-1} ; MS (ESI): m/z = 409.4 $[M+H]^+$; HRMS: m/z calcd for $\text{C}_{23}\text{H}_{25}\text{ClN}_4\text{O} + \text{H}^+$: 409.1790; found: 409.1812; HPLC: t_R = 3.83 min, purity: 97.2%.

2-Bromo-*N*-[2-(dimethylamino)ethyl]-10*H*-indolo[3,2-*b*]quinoline-11-carboxamide (3m, RMS-204): Yellow amorphous solid; mp: 237–238 °C; ^1H NMR (400 MHz, $[\text{D}_6]\text{DMSO}$): δ = 8.98 (s, 1H), 8.45 (s, 1H), 8.37 (d, J = 8.0 Hz, 1H), 8.19 (d, J = 8.8 Hz, 1H), 7.80 (d, J = 9.2 Hz, 1H), 7.68 (d, J = 7.2 Hz, 1H), 7.62 (d, J = 8.0 Hz, 1H), 7.34 (t, J = 7.6 Hz, 1H), 3.16 (m, 2H), 2.72 (m, 2H), 2.45 ppm (s, 6H); ^{13}C NMR (125 MHz, $[\text{D}_6]\text{DMSO}$): δ = 164.6, 146.7, 144.4, 141.1, 131.1, 130.6, 129.6, 129.1, 126.4, 123.8, 121.5, 120.4, 120.1, 119.3, 118.8, 111.8, 57.1, 54.8, 44.4, 36.6 ppm; IR (CHCl₃): $\tilde{\nu}_{\max}$ = 3432, 2921, 2851, 1737, 1651, 1577, 1538, 1462, 1213, 1021 cm^{-1} ; MS (ESI): m/z = 413.3 $[M+H]^+$; HRMS: m/z calcd for $\text{C}_{20}\text{H}_{19}\text{BrN}_4\text{O} + \text{H}^+$: 411.0815; found: 411.0831; HPLC: t_R = 5.43 min, purity: 100%.

***N*-[2-(Dimethylamino)ethyl]-2-fluoro-10*H*-indolo[3,2-*b*]quinoline-11-carboxamide (3n, RMS-212):** Yellow amorphous solid; mp: 187–189 °C; ^1H NMR (400 MHz, $[\text{D}_6]\text{DMSO}$): δ = 8.93 (s, 1H), 8.37 (d, J = 7.6 Hz, 1H), 8.31 (dd, J = 5.6, 9.2 Hz, 1H), 7.99 (d, J = 10.8 Hz, 1H), 7.69–7.59 (m, 3H), 7.35 (t, J = 7.6 Hz, 1H), 3.38 (m, 2H, merged with $[\text{D}_6]\text{DMSO}$), 2.67 (m, 2H), 2.42 ppm (s, 6H); ^{13}C NMR (100 MHz, $[\text{D}_6]\text{DMSO}$): δ = 164.7, 160.7 (d, $^1J_{\text{CF}}$ = 237.9 Hz), 146.1, 144.1, 140.3, 131.6, 130.3, 129.9, 123.2, 121.3, 120.6, 120.0, 119.6, 116.4 (d, $^2J_{\text{CF}}$ = 25.4 Hz), 111.8, 107.7 (d, $^2J_{\text{CF}}$ = 24.4 Hz), 57.3, 44.5, 36.8 ppm; IR (CHCl₃): $\tilde{\nu}_{\max}$ = 3440, 2920, 2850, 2090, 1633, 1460, 1338, 1215, 1021 cm^{-1} ; MS (ESI): m/z = 351.2 $[M+H]^+$; HRMS: m/z calcd for $\text{C}_{20}\text{H}_{19}\text{FN}_4\text{O} + \text{H}^+$: 351.1616; found: 351.1625; HPLC: t_R = 4.66 min, purity: 95.2%.

(2-Bromo-10*H*-indolo[3,2-*b*]quinolin-11-yl)(4-methylpiperazin-1-yl)methanone (5a, RMS-210): Yellow amorphous solid; mp: 261–262 °C; ^1H NMR (400 MHz, $[\text{D}_6]\text{DMSO}$): δ = 11.77 (s, 1H), 8.43 (d, J = 7.2 Hz, 1H), 8.35 (d, J = 5.6 Hz, 1H), 7.19 (s, 1H), 7.78–7.66 (m, 3H), 7.40 (t, J = 6.8 Hz, 1H), 4.20 (m, 1H), 3.78 (m, 1H), 3.22 (m, 2H), 2.78 (m, 1H), 2.45–2.36 (m, 2H), 2.26 (s, 3H), 2.05 ppm (m, 1H); ^{13}C NMR (100 MHz, $[\text{D}_6]\text{DMSO}$): δ = 163.6, 146.5, 144.5, 141.3, 131.3, 130.5, 130.4, 128.3, 126.8, 123.1, 122.3, 121.5, 120.5, 120.1, 118.3,

111.8, 54.9, 54.1, 46.1, 45.4, 41.2 ppm; IR (CHCl₃): $\tilde{\nu}_{\max}$ = 3404, 2920, 2850, 2806, 1616, 1490, 1470, 1446, 1397, 1338, 1295, 1252, 1230, 1195, 1170, 1145, 1109, 1062, 1032 cm⁻¹; MS (ESI): m/z = 379.1 [M + H]⁺; HRMS: m/z calcd for C₂₁H₂₀ClN₄O + H⁺: 379.1320; found: 379.1319; HPLC: t_R = 20.5 min, purity: 100%.

4-(2-Bromo-10H-indolo[3,2-b]quinoline-11-carbonyl)piperazine-1-carbaldehyde (5b, RMS-211): Yellow amorphous solid; mp: 279–280 °C; ¹H NMR (400 MHz, [D₆]DMSO): δ = 11.76 (s, 1H), 8.38 (d, J = 8.0 Hz, 1H), 8.29 (d, J = 8.4 Hz, 1H), 8.14 (d, J = 8.0 Hz, 1H), 7.92 (s, 1H), 7.72–7.60 (m, 3), 7.37 (t, J = 7.6 Hz, 1H), 4.03–3.88 (m, 2H), 3.78 (m, 1H), 3.34 (m, 2H), 3.25–3.17 ppm (m, 3H); ¹³C NMR (100 MHz, [D₆]DMSO): δ = 164.0, 161.2, 146.5, 144.5, 141.4, 131.2, 130.6, 130.5, 128.4, 126.9, 123.1, 122.4, 121.5, 120.5, 120.2, 118.0, 111.8, 46.9, 45.3, 42.0, 39.8 ppm; IR (CHCl₃): $\tilde{\nu}_{\max}$ = 3419, 2919, 1660, 1616, 1489, 1469, 1437, 1397, 1296, 1280, 1251, 1213, 1195, 1148, 1024, 1002 cm⁻¹; MS (ESI): m/z = 393.1 [M + H]⁺; HRMS: m/z calcd for C₂₁H₁₇ClN₄O₂ + H⁺: 393.1113; found: 393.1123; HPLC: t_R = 27.1 min, purity: 98.9%.

(2-Bromo-10H-indolo[3,2-b]quinolin-11-yl)(morpholino)methanone (5c, RMS-190): Yellow amorphous solid; mp: 260–262 °C; ¹H NMR (400 MHz, [D₆]DMSO): δ = 11.78 (s, 1H), 8.41 (d, J = 7.6 Hz, 1H), 8.25 (d, J = 9.2 Hz, 1H), 8.09 (s, 1H), 7.86 (d, J = 8.8 Hz, 1H), 7.73 (t, J = 7.2 Hz, 1H), 7.66 (d, J = 8.4 Hz, 1H), 7.39 (t, J = 7.2 Hz, 1H), 4.05 (m, 4H), 3.88 (m, 2H), 3.22 ppm (m, 2H); ¹³C NMR (100 MHz, [D₆]DMSO): δ = 163.8, 146.6, 146.6, 144.6, 141.5, 131.4, 130.6, 129.3, 128.3, 125.6, 123.7, 121.5, 120.5, 120.2, 119.0, 117.8, 111.8, 66.4, 65.9, 46.6, 41.8 ppm; IR (CHCl₃): $\tilde{\nu}_{\max}$ = 3416, 2921, 2852, 1615, 1488, 1468, 1440, 1397, 1337, 1304, 1271, 1234, 1213, 1192, 1147, 1112, 1059, 1028 cm⁻¹; MS (ESI): m/z = 409.9 [M + H]⁺; HRMS: m/z calcd for C₂₀H₁₆BrN₃O₂ + H⁺: 410.0499; found: 410.0495; HPLC: t_R = 32.3 min, purity: 96.9%.

(2-Fluoro-10H-indolo[3,2-b]quinolin-11-yl)(morpholino)methanone (5d, RMS-192): Yellow amorphous solid; mp: 274–275 °C; ¹H NMR (400 MHz, [D₆]DMSO): δ = 11.70 (s, 1H), 8.34 (m, 2H), 7.65 (m, 4H), 7.34 (m, 1H), 4.03–3.79 (m, 4H), 3.48 (m, 2H), 3.18 ppm (m, 2H); ¹³C NMR (125 MHz, [D₆]DMSO): δ = 163.9, 160.0 (d, ¹ J_{CF} = 223.6 Hz), 145.9, 144.3, 140.2, 132.0, 130.3, 128.4, 123.1, 121.3, 120.6, 120.1, 118.3, 116.6 (d, ² J_{CF} = 26.0 Hz), 111.8, 107.0 (d, ¹ J_{CF} = 23.0 Hz), 66.4, 65.8, 46.6, 41.7 ppm; IR (CHCl₃): $\tilde{\nu}_{\max}$ = 3429, 2920, 2851, 2350, 2089, 1626, 1516, 1494, 1478, 1442, 1398, 1338, 1306, 1272, 1215, 1197, 1149, 1111, 1068, 1031 cm⁻¹; MS (ESI): m/z = 350.1 [M + H]⁺; HRMS: m/z calcd for C₂₀H₁₆FN₃O₂ + H⁺: 350.1299; found: 350.1317; HPLC: t_R = 20.14 min, purity: 99.6%.

(10H-Indolo[3,2-b]quinolin-11-yl)(morpholino)methanone (5e, RMS-193): Yellow amorphous solid; mp: 234–235 °C; ¹H NMR (400 MHz, [D₆]DMSO): δ = 11.62 (s, 1H), 8.38 (d, J = 7.6 Hz, 1H), 8.27 (d, J = 7.6 Hz, 1H), 7.93 (d, J = 7.6 Hz, 1H), 7.67 (m, 4H), 7.33 (m, 1H), 4.03–3.79 (m, 4), 3.47 (m, 2H), 3.15 ppm (m, 2H); ¹³C NMR (125 MHz, [D₆]DMSO): δ = 164.3, 146.0, 144.4, 143.0, 130.2, 129.2, 128.0, 126.3, 126.0, 123.8, 122.3, 121.4, 120.7, 119.8, 118.9, 111.7, 66.4, 65.9, 46.7, 41.7 ppm; IR (CHCl₃): $\tilde{\nu}_{\max}$ = 3433, 2921, 2851, 1615, 1494, 1463, 1396, 1219, 1138, 1021 cm⁻¹; MS (ESI): m/z = 332.1 [M + H]⁺; HRMS: m/z calcd for C₂₀H₁₇N₃O₂ + H⁺: 332.1394; found: 332.1380; HPLC: t_R = 22.15 min, purity: 95.1%.

(S)-[2-(Hydroxymethyl)pyrrolidin-1-yl](10H-indolo[3,2-b]quinolin-11-yl)methanone (5f, RMS-194): Yellow amorphous solid; mp: 180–186 °C; ¹H NMR (400 MHz, [D₆]DMSO): δ = 11.60 (s, 1H), 11.23 (s, 1H), 8.37 (m, 1H), 8.26 (m, 1H), 7.97.83 (m, 1H), 7.78–7.58 (m, 3H), 7.31 (m, 1H), 5.07 (s, 1H), 4.40–3.88 (m, 2H), 3.00 (m, 2H), 2.07 (m, 2H), 1.87–1.67 ppm (m, 2H); ¹³C NMR (100 MHz, [D₆]DMSO): δ = 164.4, 146.2, 144.3, 143.1, 130.1, 129.2, 127.4, 126.3,

125.9, 124.6, 123.8, 121.8, 121.3, 120.7, 119.7, 111.7, 61.2, 58.8, 47.9, 27.2, 23.7 ppm; IR (CHCl₃): $\tilde{\nu}_{\max}$ = 3433, 2921, 2851, 2809, 1618, 1494, 1463, 1396, 1337, 1219, 1139, 1021 cm⁻¹; MS (ESI): m/z = 346.0 [M + H]⁺; HRMS: m/z calcd for C₂₁H₁₉N₃O₂ + H⁺: 346.1550; found: 346.1557; HPLC: t_R = 20.15 min, purity: 95.7%.

(S)-(2-Chloro-10H-indolo[3,2-b]quinolin-11-yl)[2-(hydroxymethyl)pyrrolidin-1-yl]methanone (5g, RMS-196): Yellow amorphous solid; mp: 277–278 °C; ¹H NMR (400 MHz, [D₆]DMSO): δ = 11.76 (s, 1H), 11.34 (brs, 1H), 8.37 (s, 1H), 8.28 (d, J = 8.8 Hz, 1H), 7.93 (d, J = 25.6 Hz, 1H), 7.71–7.59 (m, 3H), 7.34 (d, J = 7.2 Hz, 1H), 5.10 (s, 1H), 4.45 (m, 1H), 3.86 (m, 1H), 3.11–3.00 (m, 2H), 2.05 (m, 2H), 1.88–1.72 ppm (m, 2H); ¹³C NMR (100 MHz, [D₆]DMSO): δ = 163.7, 146.7, 144.5, 141.4, 140.5, 131.2, 130.4, 127.8, 126.7, 123.2, 122.6, 122.4, 121.4, 120.7, 120.2, 111.8, 60.6, 58.9, 48.0, 27.0, 23.6 ppm; IR (CHCl₃): $\tilde{\nu}_{\max}$ = 3429, 2923, 2082, 1633, 1465, 1405, 1215, 1022 cm⁻¹; MS (ESI): m/z = 379.1 [M]⁺, 377.1 [M – 1]⁺; HRMS: m/z calcd for C₂₁H₁₈ClN₃O₂ + H⁺: 380.1160; found: 380.1166; HPLC: t_R = 23.14 min, purity: 96.2%.

(2-Chloro-10H-indolo[3,2-b]quinolin-11-yl)(morpholino)methanone (5h, RMS-197): Yellow amorphous solid; mp: 240–241 °C; ¹H NMR (400 MHz, [D₆]DMSO): δ = 11.74 (s, 1H), 8.38 (d, J = 7.6 Hz, 1H), 8.29 (d, J = 8.8 Hz, 1H), 7.90 (s, 1H), 7.71 (dd, J = 8.4, 15.6 Hz, 2H), 7.62 (d, J = 8.0 Hz, 1H), 7.35 (t, J = 7.6 Hz, 1H), 4.06–3.92 (m, 2H), 3.87–3.79 (m, 2H), 3.50 (m, 2H), 3.19 ppm (m, 2H); ¹³C NMR (125 MHz, [D₆]DMSO): δ = 163.7, 146.5, 144.5, 141.4, 131.3, 130.6, 130.4, 128.3, 126.8, 123.1, 122.4, 121.5, 120.5, 120.2, 118.0, 111.8, 66.4, 65.8, 46.6, 41.8 ppm; IR (CHCl₃): $\tilde{\nu}_{\max}$ = 3435, 2921, 2852, 2089, 1618, 1490, 1470, 1440, 1397, 1338, 1305, 1271, 1213, 1194, 1147, 1112, 1089, 1064, 1030 cm⁻¹; MS (ESI): m/z = 366.1 [M + H]⁺; HRMS: m/z calcd for C₂₀H₁₆ClN₃O₂ + H⁺: 366.1004; found: 366.1014; HPLC: t_R = 23.28 min, purity: 97.7%.

2-Bromo-N-[4-(trifluoromethoxy)benzyl]-10H-indolo[3,2-b]quinoline-11-carboxamide (6a, RMS-158): Yellow amorphous solid; mp: 246–247 °C; ¹H NMR (400 MHz, [D₆]DMSO): δ = 11.63 (s, 1H), 9.58 (t, J = 5.6 Hz, 1H), 8.37 (d, J = 7.6 Hz, 1H), 8.20 (d, J = 8.8 Hz, 1H), 8.15 (s, 1H), 7.80 (d, J = 9.2 Hz, 1H), 7.71–7.62 (m, 4H), 7.42 (d, J = 8.0 Hz, 2H), 7.34 (t, J = 7.2 Hz, 1H), 4.74 ppm (d, J = 5.6 Hz, 2H); ¹³C NMR (100 MHz, [D₆]DMSO): δ = 164.7, 147.3, 146.8, 144.5, 141.4, 138.4, 133.1, 131.2, 130.6, 129.6, 129.0, 125.9, 123.8, 121.5, 121.0, 120.3, 120.2 (m), 119.0, 118.7, 111.9, 42.4 ppm; IR (CHCl₃): $\tilde{\nu}_{\max}$ = 3436, 2923, 2323, 1644, 1624, 1510, 1486, 1466, 1396, 1335, 1263, 1215, 1163, 1110, 1019 cm⁻¹; MS (ESI): m/z = 514.0 [M + H]⁺; HRMS: m/z calcd for C₂₄H₁₅BrF₃N₃O₂ + H⁺: 514.0406; found: 514.0425; HPLC: t_R = 37.68 min, purity: 96.2%.

2-Bromo-N-[4-(trifluoromethyl)benzyl]-10H-indolo[3,2-b]quinoline-11-carboxamide (6b, RMS-160): Yellow amorphous solid; mp: 291–292 °C; ¹H NMR (400 MHz, [D₆]DMSO): δ = 8.57 (d, J = 8.8 Hz, 1H), 8.13 (s, 1H), 8.07 (d, J = 12.0 Hz, 1H), 7.80 (s, 1H), 7.70 (d, J = 12.0 Hz, 1H), 7.63 (s, 3H), 7.58 (d, J = 8.0 Hz, 1H), 7.52 (d, J = 8.8 Hz, 1H), 7.26 (t, J = 8.0 Hz, 1H), 4.5 ppm (s, 2H); ¹³C NMR (100 MHz, [D₆]DMSO): δ = 164.8, 148.0, 146.9, 144.6, 143.7, 141.5, 131.3, 130.5, 129.1, 129.0, 128.4, 127.9, 125.9, 125.3, 122.9, 121.4, 120.4, 120.1, 118.8, 118.7, 112.0, 42.7 ppm; IR (CHCl₃): $\tilde{\nu}_{\max}$ = 3436, 2923, 2072, 1633, 1462, 1483, 1325, 1159, 1122, 1019 cm⁻¹; MS (ESI): m/z = 497.9 [M + H]⁺; HRMS: m/z calcd for C₂₄H₁₅BrF₃N₃O + H⁺: 500.0403; found: 500.0396; HPLC: t_R = 37.14 min, purity: 100%.

2-Bromo-N-[3-(trifluoromethyl)benzyl]-10H-indolo[3,2-b]quinoline-11-carboxamide (6c, RMS-162): Yellow amorphous solid; mp: 270–271 °C; ¹H NMR (400 MHz, CD₃OD): δ = 8.35 (d, J = 8.0 Hz, 1H), 8.1 (s, 1H), 8.04 (d, J = 9.2 Hz, 1H), 7.75 (s, 1H), 7.68 (m, 2H), 7.59–7.48 (m, 4H), 7.24 (t, J = 7.6 Hz, 1H), 4.78 ppm (s, 2H); ¹³C NMR

(125 MHz, [D₆]DMSO): δ = 164.8, 146.9, 144.6, 141.4, 140.4, 131.8, 131.3, 130.6, 129.5, 129.3, 129.1, 125.8, 124.0, 123.8, 121.5, 120.3, 120.1, 118.9, 118.8, 112.0, 42.6 ppm; IR (CHCl₃): $\tilde{\nu}_{\text{max}}$ = 3437, 2066, 1650, 1640, 1633, 1463, 1327, 1166, 1128, 1019 cm⁻¹; MS (ESI): m/z = 497.8 [M+H]⁺; HRMS: m/z calcd for C₂₄H₁₆BrF₃N₃O + H⁺: 500.0403; found: 500.0405; HPLC: t_R = 36.93 min, purity: 97.9%.

2-Bromo-N-[4-(trifluoromethoxy)phenyl]-10H-indolo[3,2-b]quinoline-11-carboxamide (7a, RMS-163): Yellow amorphous solid; mp: 245–247 °C; ¹H NMR (400 MHz, [D₆]DMSO): δ = 11.79 (s, 1H), 11.23 (s, 1H), 8.4 (d, J = 7.6 Hz, 1H), 8.30 (s, 1H), 8.25 (d, J = 9.2 Hz, 1H), 8.01 (d, J = 8.8 Hz, 2H), 7.85 (d, J = 9.2 Hz, 1H), 7.69 (t, J = 8.0 Hz, 1H), 7.62 (d, J = 8.0 Hz, 1H), 7.48 (d, J = 8.8 Hz, 2H), 7.36 ppm (t, J = 7.2 Hz, 1H); ¹³C NMR (100 MHz, [D₆]DMSO): δ = 163.4, 147.0, 144.6, 144.3, 141.3, 137.9, 131.2, 130.8, 129.3, 129.0, 125.7, 123.6, 121.7, 121.5, 121.4, 120.3, 120.2, 119.2, 118.8, 118.7, 111.9 ppm; IR (CHCl₃): $\tilde{\nu}_{\text{max}}$ = 3416, 2921, 2851, 1788, 1729, 1654, 1626, 11534, 1505, 1485, 1462, 1411, 1317, 1297, 1251, 1205, 1158, 1072, 1021 cm⁻¹; MS (ESI): m/z = 501.8 [M+H]⁺; HRMS: m/z calcd for C₂₃H₁₃BrF₃N₃O₂ + H⁺: 500.0216; found: 500.0234; HPLC: t_R = 39.38 min, purity: 100%.

2-Bromo-N-(4-bromophenyl)-10H-indolo[3,2-b]quinoline-11-carboxamide (7b, RMS-164): Yellow amorphous solid; mp: 242–244 °C; ¹H NMR (400 MHz, [D₆]DMSO): δ = 11.80 (s, 1H), 11.17 (s, 1H), 8.40 (d, J = 7.6 Hz, 1H), 8.27 (s, 1H), 8.25 (d, J = 9.2 Hz, 1H), 7.86 (m, 3H), 7.65 (m, 4H), 7.35 ppm (t, J = 7.2 Hz, 1H); ¹³C NMR (100 MHz, [D₆]DMSO): δ = 163.3, 147.0, 144.6, 141.3, 138.0, 131.6, 131.2, 130.8, 129.3, 128.9, 125.5, 123.6, 122.2, 121.5, 120.3, 120.2, 119.1, 118.8, 116.0, 111.9 ppm; IR (CHCl₃): $\tilde{\nu}_{\text{max}}$ = 3427, 2962, 2874, 2311, 1724, 1649, 1599, 1581, 1528, 1488, 1469, 1447, 1394, 1377, 1341, 1303, 1286, 1123, 1073, 1039 cm⁻¹; MS (ESI): m/z = 495.8 [M+H]⁺; HRMS: m/z calcd for C₂₂H₁₃Br₂N₃O + H⁺: 495.9478; found: 495.9465; HPLC: t_R = 37.7 min, purity: 95.3%.

2-Bromo-N-(4-fluorophenyl)-10H-indolo[3,2-b]quinoline-11-carboxamide (7c, RMS-165): Yellow amorphous solid; mp: 307–308 °C; ¹H NMR (400 MHz, [D₆]DMSO): δ = 11.79 (s, 1H), 11.10 (s, 1H), 8.40 (d, J = 7.6 Hz, 1H), 8.31 (s, 1H), 8.25 (d, J = 8.8 Hz, 1H), 7.91 (m, 2H), 7.85 (d, J = 8.8 Hz, 1H), 7.69 (d, J = 7.2 Hz, 1H), 7.63 (d, J = 8.0 Hz, 1H), 7.32 ppm (m, 3H); ¹³C NMR (100 MHz, [D₆]DMSO): δ = 163.0, 159.5, 157.6, 147.0, 144.7, 141.5, 135.2, 131.4, 130.6, 129.2, 128.9, 125.8, 123.7, 122.0, 121.5, 120.4, 120.2, 119.0, 115.5, 115.3, 111.9 ppm; IR (CHCl₃): $\tilde{\nu}_{\text{max}}$ = 3436, 2921, 2851, 1737, 1651, 1617, 1508, 1463, 1384, 1217, 1021 cm⁻¹; MS (ESI): m/z = 435.8 [M+H]⁺; HRMS: m/z calcd for C₂₂H₁₃BrFN₃O + H⁺: 434.0299; found: 434.0304; HPLC: t_R = 36.79 min, purity: 96.4%.

2-Aryl-10H-indolo[3,2-b]quinoline-11-carboxamides 4a–c: Pd(dppf)Cl₂ (0.2 equiv) and arylboronic acid **20** (1.2 equiv) were added to a solution of 10H-indolo[3,2-b]quinoline-C11-carboxamide **3a** (1 equiv) in 1,4-dioxane/water 50:50. The mixture was heated at reflux at 80 °C for 12 h. The solvent was evaporated, and the product was extracted with EtOAc (3 × 50 mL). The combined organic layer was dried with anhydrous sodium sulfate and was concentrated under reduced pressure. The crude product was purified by silica gel column chromatography (EtOAc/hexane) to give 2-aryl 10H-indolo[3,2-b]quinoline **4** (60–80%).

2-(4-Fluorophenyl)-N-(3-morpholinopropyl)-10H-indolo[3,2-b]quinoline-11-carboxamide (4a, RMS-128): Yellow amorphous solid; mp: 220–221 °C; ¹H NMR (400 MHz, CDCl₃): δ = 9.31 (s, 1H), 8.56 (s, 1H), 8.45 (d, J = 8.0 Hz, 1H), 8.40 (s, 1H), 8.35 (d, J = 8.5 Hz, 1H), 7.84 (d, J = 7.5 Hz, 1H), 7.67 (dd, J = 5.0, 8.0 Hz, 2H), 7.57 (t, J = 7.5 Hz, 1H), 7.42 (d, J = 8.0 Hz, 1H), 7.32 (t, J = 7.5 Hz, 1H), 7.19 (t, J = 8.5 Hz, 2H), 3.81 (m, 2H), 3.07 (m, 3H), 2.89 (m, 1H), 2.55 (m, 2H), 2.25 (m, 4H), 1.88 ppm (m, 2H); ¹³C NMR (125 MHz,

[D₆]DMSO): δ = 166.4, 163.6 (d, ¹ J_{CF} = 246.1 Hz), 147.3, 143.8, 143.5, 137.6, 131.1, 130.6, 130.4, 128.9, 128.8, 125.7, 122.5, 122.0, 121.5, 121.2, 120.7, 117.8, 116.0 (d, ² J_{CF} = 21.3 Hz), 111.3, 66.2, 58.3, 53.4, 29.7, 24.1 ppm; IR (CHCl₃): $\tilde{\nu}_{\text{max}}$ = 3436, 2066, 1650, 1633, 1464, 1019 cm⁻¹; MS (ESI): m/z = 483.1 [M+H]⁺; HRMS: m/z calcd for C₂₉H₂₇FN₄O₂ + H⁺: 483.2191; found: 483.2197; HPLC: t_R = 5.3 min, purity: 97%.

2-(3-Acetamidophenyl)-N-(3-morpholinopropyl)-10H-indolo[3,2-b]quinoline-11-carboxamide (4b, RMS-129): Yellow amorphous solid; mp: 254–256 °C; ¹H NMR (400 MHz, CDCl₃): δ = 8.30 (m, 1H), 8.24 (s, 1H), 8.19 (m, 1H), 7.92 (s, 1H), 7.86 (m, 1H), 7.53 (m, 1H), 7.48 (m, 2H), 7.36 (m, 2H), 7.23 (m, 1H), 3.62 (t, J = 6.8 Hz, 2H), 3.47 (t, J = 4.4 Hz, 4H), 2.52 (t, J = 7.2 Hz, 2H), 2.39 (s, 4H), 2.09 (s, 3H), 1.90 ppm (m, 2H); ¹³C NMR (125 MHz, CD₃OD): δ = 171.7, 168.1, 147.8, 146.1, 143.7, 142.5, 140.6, 139.5, 131.7, 130.1, 130.5, 129.7, 127.3, 124.2, 124.1, 122.9, 122.8, 121.9, 121.7, 121.3, 120.3, 120.0, 112.7, 67.3, 57.8, 54.5, 39.5, 26.7, 24.0 ppm; IR (CHCl₃): $\tilde{\nu}_{\text{max}}$ = 3436, 2921, 2851, 2066, 1639, 1464, 1019 cm⁻¹; MS (ESI): m/z = 522.1 [M+H]⁺; HRMS: m/z calcd for C₃₁H₃₁N₅O₃ + H⁺: 522.2500; found: 522.2507; HPLC: t_R = 8.37 min, purity: 98.6%.

2-(4-Acetylphenyl)-N-(3-morpholinopropyl)-10H-indolo[3,2-b]quinoline-11-carboxamide (4c, RMS-130): Yellow amorphous solid; mp: 226–228 °C; ¹H NMR (400 MHz, CDCl₃): δ = 9.27 (s, 1H), 8.58 (m, 2H), 8.49 (d, J = 7.6 Hz, 1H), 8.42 (d, J = 8.8 Hz, 1H), 8.10 (d, J = 8.0 Hz, 2H), 7.94 (d, J = 8.8 Hz, 1H), 7.83 (d, J = 8.0 Hz, 2H), 7.60 (t, J = 7.6 Hz, 1H), 7.43 (d, J = 8.0 Hz, 1H), 7.35 (t, J = 7.2 Hz, 1H), 3.82 (m, 2H), 3.0 (s, 4H), 2.67 (s, 3H), 2.51 (t, J = 6.0 Hz, 2H), 2.19 (m, 4H), 1.86 ppm (m, 2H); ¹³C NMR (100 MHz, CD₃OD): δ = 166.9, 164.7, 146.7, 144.5, 142.8, 135.8, 131.6, 131.5, 130.3, 130.0, 129.1, 129.0, 128.6, 127.2, 125.2, 122.7, 122.5, 121.3, 120.9, 120.6, 119.8, 111.9, 66.1, 56.1, 53.3, 37.8, 27.1, 18.8 ppm; IR (CHCl₃): $\tilde{\nu}_{\text{max}}$ = 3436, 2924, 2856, 1647, 1620, 1401, 1269, 1019 cm⁻¹; MS (ESI): m/z = 507.1 [M+H]⁺; HRMS: m/z calcd for C₃₁H₃₀N₄O₃ + H⁺: 507.2391; found: 507.2391; HPLC: t_R = 5.34 min, purity: 95.6%.

Biological methods

Measurement of inhibition of *P. falciparum* growth in culture.^[27]

In this study, CQ-sensitive 3D7 and CQ-resistant Dd2 and Indo strains of *P. falciparum* were cultivated in vitro by the method of Trager and Jensen^[28] with minor modifications. Cultures were maintained in fresh O⁺ human erythrocytes at 4% hematocrit in complete medium (RPMI 1640 with 0.2% sodium bicarbonate, 0.5% Al-bumax, 45 mg L⁻¹ hypoxanthine, and 50 mg L⁻¹ gentamicin) at 37 °C under reduced O₂ (gas mixture 5% O₂, 5% CO₂, and 90% N₂). Stock solutions of chloroquine were prepared in water (Milli-Q grade). Test compounds were dissolved in DMSO. All stocks were then diluted with culture medium to achieve the required concentrations (in all cases, the final concentration of DMSO was 0.4%, which was found to be nontoxic to the parasite). Compounds were then placed in 96-well flat-bottomed tissue culture grade plates to yield triplicate wells with drug concentrations ranging from 0 to 100 μ M in a final well volume of 100 μ L for primary screening. The antimalarial activity of the compounds was measured by the fluorescence-based SYBR green I assay against CQ-sensitive and CQ-resistant strains.^[29] Parasite culture was synchronized at the ring stage with 5% sorbitol. Synchronized culture was aliquoted to a drug containing 96-well plates at 2% hematocrit and 1% parasitemia. After 48 h of incubation under standard culture conditions, plates were harvested and read by the SYBR green I fluorescence-based method by using a 96-well fluorescence plate reader (Victor, PerkinElmer), with excitation and emission wavelengths at 485 and

530 nm, respectively. The fluorescence readings were plotted against drug concentration, and the IC_{50} values were obtained by visual matching of the drug concentration giving 50% inhibition of growth. ICEstimator 1.2 online software was also used to calculate the IC_{50} and IC_{90} values.

In vitro cytotoxicity in mammalian cell lines: Animal cell lines (HUH-7 and HEK-293T) were used to determine drug toxicity by using the MTT assay.^[30] HUH-7 and HEK-293T cells were cultured in complete RPMI containing 10% fetal bovine serum, 0.2% sodium bicarbonate, and $50 \mu\text{g mL}^{-1}$ gentamicin. Briefly, cells (10^4 cells per $200 \mu\text{L}$ per well) were seeded into 96-well flat-bottomed tissue-culture plates in complete culture medium. Compound solutions (in all cases, the final concentration of DMSO was 0.4%) were added after overnight seeding and were incubated for 24 h in a humidified atmosphere at 37°C and 5% CO_2 . DMSO (final concentration: 10%) was added as a positive control. An aliquot of a stock solution of 3-(4,5-dimethylthiazol-2-yl)-2,5-diphenyltetrazolium bromide (MTT) (5 mg mL^{-1} in $1 \times$ phosphate-buffered saline) was added at $20 \mu\text{L}$ per well, and the samples were incubated for another 3 h. After spinning the plate at 1500 rpm for 5 min, supernatant was removed and $100 \mu\text{L}$ of the stock agent DMSO was added to each well. Formation of formazan, an index of growth, was read at $\lambda = 570 \text{ nm}$ by a 96-well plate reader (Versa Max), and the IC_{50} values were determined by analysis of dose–response curves. Selectivity index was calculated as $IC_{50(\text{mammalian cell})}/IC_{50(\text{P3D7})}$.

Aqueous solubility, hrCYP P450 isoenzyme inhibition, and Caco-2 permeability: The thermodynamic aqueous solubility in PBS (pH 7.4), SGF (pH 1.2), and SIF (pH 6.8) was determined by using a protocol described earlier.^[31] The hrCYP P450 inhibition of five major isoenzymes, CYP3A4, CYP2D6, CYP2C9, CYP2C19, and CYP1A2, was determined at $10 \mu\text{M}$ as described earlier.^[32] Similarly, the caco-2 permeability study was conducted as described earlier.^[32]

Microscopic evaluation of the stage-specific kill kinetics of 3g against *P. falciparum* stages: To find if there was stage specificity in the action of **3g**, highly synchronized P3D7 cultures at ring (R), trophozoite (T), and schizont (S) stages were treated with **3g** at the IC_{90} value ($3.5 \mu\text{M}$) by the drug pressure followed by drug withdrawal method as described below. The ring-stage *P. falciparum* culture was tightly synchronized for two continuous life cycles by using 5% sorbitol to maintain the synchronicity of the *Plasmodium* stages, and the synchrony of each stage was confirmed by microscopy. One percent of synchronized early rings (0–6 h), early trophozoites ($\approx 24 \text{ h}$ post-synchronization), and early schizonts ($\approx 40 \text{ h}$ post-synchronization) was used for the stage-specific drug-action studies. Ring-stage cultures were treated with the test sample at the IC_{90} value for 12, 24, 36, and 48 h. Similarly, trophozoite-stage (3, 6, 18, and 24 h) and schizont-stage (3, 6, and 12 h) cultures were treated with the test sample at the IC_{90} value. Following drug treatment, as indicated above, the drugs were withdrawn by centrifugal removal of conditioned medium followed by media wash. The washed cells were maintained under standard culture conditions in drug-free cRPMI medium for a total of 96, 72, and 60 h for ring, trophozoites, and schizonts, respectively. The percentage of stage-specific inhibition of each treatment was calculated in comparison with drug-free control by microscopic counting of 3000 cells for each stage. Parasitized and non-parasitized cells were counted by using *Plasmodium* auto count 0.1 software developed by Ma et al.^[33] The parasites with pycnotic morphology were considered as nonviable cells.

Kinetics of 3g uptake by malaria parasite: Trophozoite-stage-enriched P3D7 culture ($\approx 4\%$ parasitemia and 2% hematocrit, $200 \mu\text{L}$) was incubated with **3g** ($50 \mu\text{M}$) at 37°C for different time points (15 min to 6 h). After incubation for each time point, the culture was washed twice with $1 \times$ PBS ($500 \mu\text{L}$) by using centrifugation (1500 RPM, 2 min) and was reconstituted in $100 \mu\text{L}$ $1 \times$ PBS. Wet mount of each sample was observed under fluorescence (DAPI filter) and optical microscopy.

Colocalization of fluorescence from 3g (blue) with EtBr/Lyso-Tracker (red): The parasite cultures were incubated with test compounds ($50 \mu\text{M}$) for 3 h. After incubation, the cells were washed with $1 \times$ PBS by centrifugation (1500 rpm, 2 min). Further, the washed cells were incubated with EtBr stain ($10 \mu\text{g mL}^{-1}$, Sigma), a DNA binding stain that emits red fluorescence, and LysoTracker red (50 nM), a fluorophore that accumulates in acidic cell organelles such as food vacuoles in separate experiments for 30 min at 37°C . The cells were washed twice with $1 \times$ PBS ($500 \mu\text{L}$) by centrifugation (1500 rpm, 2 min) and were reconstituted in $1 \times$ PBS ($100 \mu\text{L}$). After washing, wet mount of each sample was prepared and observed under fluorescence and optical microscopy.

Inhibition of detergent-mediated β -hematin formation assay: The detergent-mediated β -hematin formation method was adopted as previously described by Sandlin et al.^[22a] with minor modifications. A hemin solution (25 mM) was prepared by dissolving hemin (Fluka, Switzerland) in DMSO, and the solution was filtered through a $0.22 \mu\text{m}$ membrane syringe filter. This stock solution was diluted by vortexing to prepare a $228 \mu\text{M}$ hemin suspension in 2 M acetate buffer (pH 4.9). A $348 \mu\text{M}$ solution of NP–40 (Fluka, Switzerland) was prepared in Sterile and filtered Milli-Q water. Stock solutions of chloroquine (CQ, 50 mM) and test compounds (25 mM) were prepared in water and DMSO, respectively. The stocks of CQ and test compounds were diluted in their respective solvents to achieve the required concentrations. In all cases, the final concentration of DMSO was 4% (v/v), which showed no effect on β -hematin formation. Test compounds ($4 \mu\text{L}$) were then placed in triplicate wells of 96-well flat-bottomed plates followed by water ($31.25 \mu\text{L}$), NP–40 solution ($8.75 \mu\text{L}$), acetone ($12.25 \mu\text{L}$), and heme suspension ($43.75 \mu\text{L}$) in a final well volume of $100 \mu\text{L}$. The final concentrations of the test compounds/CQ were 0, 125, 250, 500, 750, and $1000 \mu\text{M}$, whereas additional concentrations up to 2 mM were tested for CQ. Further, the plates were incubated (6 h) in a shaking incubator (37°C , 50 rpm), following which the samples in the wells were processed by using the pyridine–ferrochrome method by adding acetone ($26.25 \mu\text{L}$) and pyridine solution [(50% pyridine, 20% acetone, and 200 mM HEPES, pH 7.4 in water)] ($14 \mu\text{L}$). Then, the plates were kept under shaking for 30 min to dissolve the free heme. After incubation, the plates were read at $\lambda = 405 \text{ nm}$ by using a SpectraMax multiwell plate reader. Inhibition of β -hematin formation by test compounds was assessed by comparing the positive (CQ) and negative controls (4% DMSO). Finally, dose–response curves were generated to calculate the IC_{50} values of the test compounds.

Inhibition of hemoglobin uptake by 3g: Synchronized trophozoite-stage (28 h post-invasion) *P. falciparum* 3D7 cultures (4% parasitemia, 2% hematocrit) were treated with the IC_{90} value of **3g** ($3.5 \mu\text{M}$) for 15 h. The relative hemoglobin contents of treated and untreated PRBCs were determined at A_{540} by following sorbitol-mediated hemolysis. Identical amounts of treated and untreated parasitized cultures ($50 \mu\text{L}$ PCV) were subjected to sorbitol treatment ($50 \mu\text{L}$ PCV with $200 \mu\text{L}$ sorbitol, 10 min, 37°C) to enable hemolysis. Thereafter, samples were centrifuged (400 g, 5 min) and supernatants were aspirated into fresh microfuge tubes. Further,

the supernatant was centrifuged (2200 g, 7 min) to remove erythrocyte ghosts. The supernatants were then transferred to wells of a 96-well plate, and absorbance of released hemoglobin was estimated at $\lambda = 540$ nm by using an ELISA plate reader

FACS analysis of inhibition of FITC-dextran endocytosis by malaria parasite

1) Preparation of FITC-dextran-loaded resealed RBCs: The endocytosis process of *Plasmodium* was measured by using parasites infected into FITC-dextran-resealed RBCs. FITC-dextran-resealed RBCs were obtained by incubating RBCs in four volumes of ice-cold hypotonic buffer [sodium phosphate buffer (5 mM, pH 7.5), Mg-ATP (1 mM) and FITC-dextran (50 μ M)] for 10 min. NaCl was added to a final concentration of 0.15 M; incubation done for 45 min at 37 °C to allow resealing.^[34] The resealed cells were washed with RPMI (2 \times) and were stored at 4 °C. The incorporation of FITC-dextran into the RBCs was evident from the bright-green fluorescent cells observed by fluorescence microscopy.

2) Isolation of late-stage parasites and incubation with FITC-dextran-loaded resealed RBCs: Late-stage parasites isolated by using 60% percol^[35] were incubated with resealed RBCs to facilitate their invasion by merozoites.

3) Measurement of the effect of 3g on endocytosis: After invasion, the 18 and 24 h cultures were incubated with or without 3g (IC₉₀: 3.5 μ M) for 6 h each. After 6 h of incubation, all the cultures were subjected to saponin (0.025% w/v) lysis to release parasites from RBCs. Further the released parasites were washed twice with PBS and re-suspended in PBS for measurement of endocytosed FITC-dextran by FACS analysis.

Pharmacokinetic analysis: The pharmacokinetic properties of 3g were evaluated in male BALB/c mice following a single 10 mg kg⁻¹ oral dose or 1 mg kg⁻¹ intravenous (i.v.) dose. For oral dose, 3g was taken in normal saline containing Tween 80 and 0.5% (w/v) methyl cellulose. The i.v. dose of 3g was prepared by taking it in a mixture of DMSO/(solutol/absolute alcohol = 1:1, v/v)/normal saline = 5:5:90 (v/v). Formulations were made on the same day of dosing and were kept at room temperature. Prepared drug formulations were administered to mice groups (12 mice per group) by appropriate routes. After dosing, plasma samples were collected from mice blood samples for 0–24 h. To extract the compounds from the plasma sample, *tert*-butyl methyl ether (1.5 mL) was added to plasma (50 μ L), and the sample was vortexed for 5 min. Then, the samples were centrifuged (14000 rpm, 5 min, 4 °C). After centrifugation, the organic layer of the samples were separated into a fresh tube and dried. The residues were reconstituted in acetonitrile. Then, the samples were analyzed by LC-MS/MS by using an Atlantis dC18 column [4.6 \times 50 mm, 3 μ m (Waters)] and a gradient of 0.2% formic acid and acetonitrile as the mobile phase. Further, the results were analyzed for pharmacokinetic parameters by using the WinNonlin 5.3 software package.

In vivo antimalarial activities of 3g in a *P. berghei* infected mouse model of malaria: The curative antimalarial potency of 3g was evaluated in a *Plasmodium berghei* (ANKA) infected mouse model of malaria, as described earlier by Ryley and Peters.^[36] All mice (BALB/c, female, 5–6 weeks, 22–25 g) were infected with 10⁵ parasitized RBCs through intravenous (i.v.) injection. After infection, the mice were divided into three groups ($n = 5$ /group): 1) vehicle control, 2) positive control (chloroquine, 10 mg kg⁻¹ body weight), and 3) test compound (50 mg kg⁻¹ body weight). After 24 h of infection, 3g in 200 μ L solution was orally administered to each mouse for four consecutive days (single dose per day). For dosing,

weighed compounds were wetted with Tween 80 (2% final concentration) and were triturated in a mortar and pestle; then, 2% hydroxypropyl methylcellulose in normal saline was slowly added to make up a final volume of 1.1 mL. From this solution, each mouse was administered 200 μ L. Drug formulations were made on each day of dosing. The control group was administered with 200 μ L of vehicle solution [2% hydroxypropyl methylcellulose with 2% Tween 80 in normal saline]. All the mice groups were monitored daily for their behavior. From the fifth day onward, thin blood smears were prepared every alternate day till the end of the experiment by using a drop of tail blood. Further, the blood smears were stained with Giemsa and were evaluated under microscope for percentage of parasitemia.

Abbreviations

CQ: chloroquine, Pf: *Plasmodium falciparum*, CYP: cytochrome P450, SI: selectivity index, FBS: fetal bovine serum, PBS: phosphate-buffered saline, FCS: fetal calf serum, SGF: simulated gastric fluid, SIF: simulated intestinal fluid, HRMS (ESI): high-resolution electrospray ionization mass spectrometry, HPMC: hydroxypropyl methylcellulose.

Acknowledgements

R.M. thanks the Council of Scientific & Industrial Research (CSIR) for a research fellowship. The authors are thankful to the Analytical Department, Indian Institute of Integrative Medicine (IIIM) for analytical support. The chemistry work was supported by the CSIR 12th FYP grant BSC-0205 and CSIR-Young Scientist Grant (P-81–113). The authors declare no competing financial interest.

Keywords: alkaloids • antimalarial agents • fused-ring systems • hemoglobin • parasites

- [1] *World Malaria Report 2016*, World Health Organization: <http://www.who.int/malaria/publications/world-malaria-report-2016/report/en/>, ISBN 978-924-151171-1, 2016 (accessed November 5, 2018).
- [2] a) K. I. Barnes, N. J. White, *Acta Trop.* **2005**, *94*, 230–240; b) F. B. Augusto, *Bull. Math. Biol.* **2014**, *76*, 1607–1641.
- [3] a) E. L. Flannery, A. K. Chatterjee, E. A. Winzeler, *Nat. Rev. Microbiol.* **2013**, *11*, 849–862; b) M. Schlitzer, *Arch. Pharm. Chem. Life Sci.* **2008**, *341*, 149–163; c) A. C. Aguiar, E. M. Rocha, N. B. Souza, T. C. Franca, A. U. Krettli, *Mem. Inst. Oswaldo Cruz* **2012**, *107*, 831–845; d) E. A. Ashley, A. P. Phyto, *Drugs* **2018**, *78*, 861–879; e) M. A. Biamonte, J. Wanner, K. G. Le Roch, *Bioorg. Med. Chem. Lett.* **2013**, *23*, 2829–2843; f) M. Medebielle, *Curr. Top. Med. Chem.* **2014**, *14*, 1635–1636.
- [4] a) O. Taglialatela-Scafati, *Future Med. Chem.* **2014**, *6*, 365–367; b) G. Alebie, B. Urga, A. Worku, *Malar. J.* **2017**, *16*, 307.
- [5] a) F. Macintyre, Y. Adoke, A. B. Tiono, T. T. Duong, G. Mombo-Ngoma, M. Bouyou-Akotet, H. Tinto, Q. Bassat, S. Issifou, M. Adamy, H. Demarest, S. Duparc, D. Leroy, B. E. Laurijssens, S. Bigenet, A. Kibuuka, A. K. Tshetu, M. Smith, C. Foster, I. Leipoldt, P. G. Kremsner, B. Q. Phuc, A. Ouedraogo, M. Ramharter, O. Z.-Piperaquine Study Group, *BMC Med.* **2017**, *15*, 181; b) P. Amoa Onguene, F. Ntie-Kang, L. Lifongo, J. Ndom, W. Sippl, L. Mbaze, *Malar. J.* **2013**, *12*, 449; c) O. A. Toure, N. Valecha, A. K. Tshetu, R. Thompson, S. Krudsood, O. Gaye, B. H. K. Rao, I. Sagara, T. K. Bose, S. Mohanty, B. S. Rao, A. R. Anvikar, V. Mwapasa, H. Noedl, S. Arora, A. Roy, S. S. Iyer, P. Sharma, N. Saha, R. K. Jalali, A.-P. S. Team, L. Tiachoh, S. Enosse, N. Tangpukdee, J. Kokolomami, J. L. Ndiaye, D. Rao, N. N. Yumva, B. Sidibe, R. Mohanty, A. C. Jha, M. Nyirenda, P. Starzengruber, P. Swoboda, *Clin. Infect. Dis.* **2016**, *62*, 964–971.
- [6] a) D. Dwuma-Badu, J. S. Ayim, N. I. Fiagbe, J. E. Knapp, P. L. Schiff, Jr., D. J. Slatkin, *J. Pharm. Sci.* **1978**, *67*, 433–434; b) K. Cimanga, T. De

- Bruyne, L. Pieters, M. Claeys, A. Vlietinck, *Tetrahedron Lett.* **1996**, *37*, 1703–1706.
- [7] "The Golden Roots of *Cryptolepis sanguinolenta*" A. A. Appiah in *African Natural Plant Products: New Discoveries and Challenges in Chemistry and Quality (ACS Symposium Series)*, American Chemical Society, Washington, DC, **2009**, Vol. 1021, pp. 231–239.
- [8] a) E. Delvaux, *J. Pharm. Belg.* **1931**, *13*, 973–976; b) E. Clinquant, *Bull. Acad. R. Med. Belg.* **1929**, *12*, 627–635.
- [9] E. Gellért, R. Hamet, E. Schlittler, *Helv. Chim. Acta* **1951**, *34*, 642–651.
- [10] a) K. Cimanga, T. De Bruyne, L. Pieters, A. J. Vlietinck, C. A. Turge, *J. Nat. Prod.* **1997**, *60*, 688–691; b) P. Grellier, L. Ramiarmanana, V. Millerioux, E. Deharo, J. Schrevel, F. Frappier, F. Trigalo, B. Bodo, J.-L. Poussot, *Phytother. Res.* **1996**, *10*, 317–321; c) O. Onyeibor, S. L. Croft, H. I. Dodson, M. Feiz-Haddad, H. Kendrick, N. J. Millington, S. Parapini, R. M. Phillips, S. Seville, S. D. Shnyder, D. Taramelli, C. W. Wright, *J. Med. Chem.* **2005**, *48*, 2701–2709; d) C. W. Wright, J. Addae-Kyereme, A. G. Breen, J. E. Brown, M. F. Cox, S. L. Croft, Y. Gokcek, H. Kendrick, R. M. Phillips, P. L. Pollet, *J. Med. Chem.* **2001**, *44*, 3187–3194.
- [11] J. N. Lisgarten, M. Coll, J. Portugal, C. W. Wright, J. Aymami, *Nat. Struct. Mol. Biol.* **2002**, *9*, 57–60.
- [12] D. E. Bierer, L. G. Dubenkov, P. Zhang, Q. Lu, P. A. Imbach, A. W. Garofalo, P.-W. Phuan, D. M. Fort, J. Litvak, R. E. Gerber, B. Sloan, J. Luo, R. Cooper, G. M. Reaven, *J. Med. Chem.* **1998**, *41*, 2754–2764.
- [13] S. Y. Ablordeppey, P. Fan, S. Li, A. M. Clark, C. D. Hufford, *Bioorg. Med. Chem.* **2002**, *10*, 1337–1346.
- [14] X. Y. Zhu, L. G. Mardenborough, S. Li, A. Khan, W. Zhang, P. Fan, M. Jacob, S. Khan, L. Walker, S. Y. Ablordeppey, *Bioorg. Med. Chem.* **2007**, *15*, 686–695.
- [15] T.-M. Ou, Y.-J. Lu, C. Zhang, Z.-S. Huang, X.-D. Wang, J.-H. Tan, Y. Chen, D.-L. Ma, K.-Y. Wong, J. C.-O. Tang, A. S.-C. Chan, L.-Q. Gu, *J. Med. Chem.* **2007**, *50*, 1465–1474.
- [16] a) Y.-J. Lu, T.-M. Ou, J.-H. Tan, J.-Q. Hou, W.-Y. Shao, D. Peng, N. Sun, X.-D. Wang, W.-B. Wu, X.-Z. Bu, Z.-S. Huang, D.-L. Ma, K.-Y. Wong, L.-Q. Gu, *J. Med. Chem.* **2008**, *51*, 6381–6392; b) E. Arzel, P. Rocca, P. Grellier, M. Labaied, F. Frappier, F. Gueritte, C. Gaspard, F. Marsais, A. Godard, G. Queguiner, *J. Med. Chem.* **2001**, *44*, 949–960.
- [17] a) J. Lavrado, G. G. Cabal, M. Prudencio, M. M. Mota, J. Gut, P. J. Rosenthal, C. Diaz, R. C. Guedes, D. J. V. A. dos Santos, E. Bichenkova, K. T. Douglas, R. Moreira, A. Paulo, *J. Med. Chem.* **2011**, *54*, 734–750; b) J. Lavrado, A. Paulo, J. Gut, P. J. Rosenthal, R. Moreira, *Bioorg. Med. Chem. Lett.* **2008**, *18*, 1378–1381.
- [18] L. F. Rocha e Silva, A. Montoia, R. C. Amorim, M. R. Melo, M. C. Henrique, S. M. Nunomura, M. R. Costa, V. F. Andrade Neto, D. S. Costa, G. Dantas, J. Lavrado, R. Moreira, A. Paulo, A. C. Pinto, W. P. Tadei, R. S. Zacardi, M. N. Eberlin, A. M. Pohlit, *Phytomedicine* **2012**, *20*, 71–76.
- [19] Q. Huang, W. L. Fu, *Clin. Chem. Lab. Med.* **2005**, *43*, 841–842.
- [20] R. Howe, M. Kelly, J. Jimah, D. Hodge, A. R. Odom, *Eukaryotic Cell* **2013**, *12*, 215–223.
- [21] a) C. D. Fitch, *Life Sci.* **2004**, *74*, 1957–1972; b) A. C. de Dios, R. Tycko, L. M. B. Ursos, P. D. Roepe, *J. Phys. Chem. A* **2003**, *107*, 5821–5825; c) A. P. Gorka, A. de Dios, P. D. Roepe, *J. Med. Chem.* **2013**, *56*, 5231–5246; d) I. Solomonov, M. Osipova, Y. Feldman, C. Baetz, K. Kjaer, I. K. Robinson, G. T. Webster, D. McNaughton, B. R. Wood, I. Weissbuch, L. Leiserowitz, *J. Am. Chem. Soc.* **2007**, *129*, 2615–2627.
- [22] a) R. D. Sandlin, M. D. Carter, P. J. Lee, J. M. Auschwitz, S. E. Leed, J. D. Johnson, D. W. Wright, *Antimicrob. Agents Chemother.* **2011**, *55*, 3363–3369; b) R. D. Sandlin, K. Y. Fong, K. J. Wicht, H. M. Carrell, T. J. Egan, D. W. Wright, *Int. J. Parasitol. Drugs Drug Resist.* **2014**, *4*, 316–325.
- [23] T. H. Jonckers, S. van Miert, K. Cimanga, C. Bailly, P. Colson, M. C. De Pauw-Gillet, H. van den Heuvel, M. Claeys, F. Lemiere, E. L. Esmans, J. Rozenski, L. Quirijnen, L. Maes, R. Dommissie, G. L. Lemiere, A. Vlietinck, L. Pieters, *J. Med. Chem.* **2002**, *45*, 3497–3508.
- [24] a) C. Lambros, J. P. Vanderberg, *J. Parasitol.* **1979**, *65*, 418–420; b) M. L. Go, M. Liu, P. Wilairat, P. J. Rosenthal, K. J. Saliba, K. Kirk, *Antimicrob. Agents Chemother.* **2004**, *48*, 3241–3245.
- [25] a) H. Ginsburg, S. Kutner, M. Krugliak, Z. I. Cabantchik, *Mol. Biochem. Parasitol.* **1985**, *14*, 313–322; b) K. Kirk, H. A. Horner, B. C. Elford, J. C. Ellory, C. I. Newbold, *J. Biol. Chem.* **1994**, *269*, 3339–3347.
- [26] J. M. Mauritz, A. Esposito, H. Ginsburg, C. F. Kaminski, T. Tiffert, V. L. Lew, *PLoS Comput. Biol.* **2009**, *5*, e1000339.
- [27] N. Sharma, D. Mohanakrishnan, U. K. Sharma, R. Kumar, A. K. Sinha, D. Sahal, *Eur. J. Med. Chem.* **2014**, *79*, 350–368.
- [28] W. Trager, J. B. Jensen, *Science* **1976**, *193*, 673–675.
- [29] M. Smilkstein, N. Sriwilaijaroen, J. X. Kelly, P. Wilairat, M. Riscoe, *Antimicrob. Agents Chemother.* **2004**, *48*, 1803–1806.
- [30] T. Mosmann, *J. Immunol. Methods* **1983**, *65*, 55–63.
- [31] S. S. Bharate, R. A. Vishwakarma, *Bioorg. Med. Chem. Lett.* **2015**, *25*, 1561–1567.
- [32] a) S. B. Bharate, V. Kumar, S. K. Jain, M. J. Mintoo, S. K. Guru, V. K. Nuthakki, N. Sharma, S. S. Bharate, S. G. Gandhi, D. M. Mondhe, S. Bhushan, R. A. Vishwakarma, *J. Med. Chem.* **2018**, *61*, 1664–1687; b) S. Mahale, S. B. Bharate, S. Manda, P. Joshi, S. S. Bharate, P. R. Jenkins, R. A. Vishwakarma, B. Chaudhuri, *J. Med. Chem.* **2014**, *57*, 9658–9672.
- [33] C. Ma, P. Harrison, L. Wang, R. L. Coppel, *Malar. J.* **2010**, *9*, 348.
- [34] a) A. R. Dluzewski, K. Rangachari, R. J. Wilson, W. B. Gratzner, *Mol. Biochem. Parasitol.* **1983**, *9*, 145–160; b) S. Frankland, A. Adisa, P. Horrocks, T. F. Taraschi, T. Schneider, S. R. Elliott, S. J. Rogerson, E. Knuepfer, A. F. Cowman, C. I. Newbold, L. Tilley, *Eukaryotic Cell* **2006**, *5*, 849–860; c) N. Klonis, M. P. Crespo-Ortiz, I. Bottova, N. Abu-Bakar, S. Kenny, P. J. Rosenthal, L. Tilley, *Proc. Natl. Acad. Sci. USA* **2011**, *108*, 11405–11410.
- [35] M. Wahlgren, K. Berzins, P. Perlmann, A. Bjorkman, *Clin. Exp. Immunol.* **1983**, *54*, 127–134.
- [36] J. F. Ryley, W. Peters, *Ann. Trop. Med. Parasitol.* **1970**, *64*, 209–222.

Manuscript received: August 27, 2018

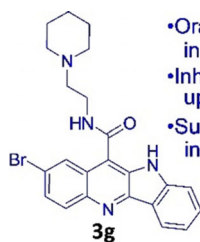
Revised manuscript received: October 10, 2018

Accepted manuscript online: October 24, 2018

Version of record online: ■■■ 0000

FULL PAPERS

Bug out: The discovery of orally bio-available compound **3g** possessing promising in vitro and in vivo antimalarial activity is reported. Compound **3g** targets the food vacuole of the parasite, inhibits the uptake of host hemoglobin, and also inhibits the basic endocytic processes of the parasite. In a *Plasmodium berghei* (ANKA)-infected mouse model of malaria, mice treated with **3g** show suppression of parasitemia and increased life span.



- Orally effective antimalarial indoloquinoline
- Inhibits host hemoglobin uptake
- Suppresses parasitemia in mice model

Pf3D7: IC₅₀ = 1.3 μM
PfDd2: IC₅₀ = 6.3 μM
PfIndo: IC₅₀ = 5 μM

R. Mudududdla, D. Mohanakrishnan, S. S. Bharate, R. A. Vishwakarma, D. Sahal,* S. B. Bharate*

■■■ – ■■■

Orally Effective Aminoalkyl 10H-Indolo[3,2-*b*]quinoline-11-carboxamide Kills the Malaria Parasite by Inhibiting Host Hemoglobin Uptake

